Journal of Medicinal Chemistry

Article

pubs.acs.org/jmc

# Influence of Neighboring Groups on the Thermodynamics of Hydrophobic Binding: An Added Complex Facet to the Hydrophobic Effect

Nader N. Nasief* and David Hangauer*

Department of Chemistry, University at Buffalo, The State University of New York, Buffalo, New York 14260, United States

Supporting Information

**ABSTRACT:** The thermodynamic consequences of systematic modifications in a ligand side chain that binds in a shallow hydrophobic pocket, in the presence and absence of a neighboring ligand carboxylate group, were evaluated using isothermal titration calorimetry (ITC). Data revealed that the carboxylate significantly changes the relative thermodynamic signatures of these modifications, likely via altering the H-bonding/organization status of the hydration waters both in the unbound and the bound states. This carboxylate group was found to be proenthalpic, antientropic in some cases, and antienthalpic, proentropic in others. A remarkable enthalpy–entropy compensation relationship was also observed, reflecting the fact that the hydrophobic effect is governed by the thermodynamic status of the associated aqueous environment. This study could improve our understanding of the hydrophobic effect and may enhance our ability to design potent ligands that are capable of modulating biological processes.

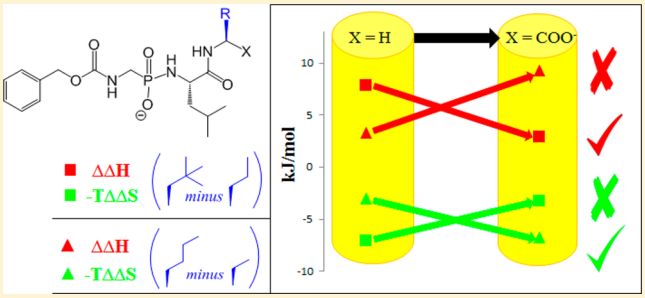


## INTRODUCTION

The hydrophobic effect is one of the major driving forces for molecular recognition and ligand–protein binding. In the realm of ligand–protein binding, the hydrophobic effect denotes the tendency of the ligand hydrophobic groups to associate with the protein hydrophobic pockets to decrease the hydrophobic surface exposed to the aqueous phase (assuming the ligand's hydrophobic moieties and their protein binding pockets have the necessary shape complementarity). This decrease in the hydrophobic surface at the ligand–protein/water interface has long been viewed as being associated with favorable entropic changes caused by the increase in the mobility of structured water molecules upon their release from the hydrophobic interface to the bulk water.[1,2] These favorable entropic changes, in turn, have been considered the cause of the favorable free energy and the spontaneity of the hydrophobic associations. The entropically driven hydrophobic effect was alternatively explained in terms of hydrophobic hydration, which is accompanied by large entropy loss that decreases as hydrophobic solutes aggregate. This large entropy loss is a result of the solvent-excluded volume effect caused by the creation of a cavity to host the hydrophobic solute.[3−5]

The view of the hydrophobic effect being driven only by favorable entropy is, however, incomplete. For example, recent studies have shown that hydrophobic associations may be driven by favorable enthalpic changes as well.[6−11] This enthalpically driven hydrophobic binding was often termed "nonclassical hydrophobic effect". In the case of the MUP protein, this hydrophobic effect was attributed to the dispersion interactions between the ligand hydrophobic group and a suboptimally hydrated protein pocket.[8] In other cases, the displacement of disordered water molecules from the protein hydrophobic pockets was invoked to rationalize the enthalpic signal caused by this hydrophobic binding.[9−11] In a recent study, the binding of a series of phosphonamidate ligands with different P2′ hydrophobic side chains to thermolysin (TLN), a Zn-endopeptidase obtained from *Bacillus thermoproteolyticus*,[12−14] was investigated by high resolution X-ray crystallography.[15] These hydrophobic side chains bind in the S2′ pocket which is a shallow, flat and solvent-exposed hydrophobic pocket (Figure 1). This study revealed much about the hydration status of this pocket and the water molecules that are displaced by the investigated hydrophobic side chains. It was also shown that the thermodynamic signature of the binding of these side chains is likely correlated with the water displacement/reorganization pattern in the S2′ pocket. The molecular origin of the hydrophobic effect is therefore too complicated to be confined to one or two models which attempt to attribute it to a single major event that dominates each hydrophobic association. This complexity, together with the relative lack of experimental techniques that detect the molecular changes taking place upon hydrophobic association, particularly changes in the dynamics of the hydration waters, causes the hydrophobic binding phenomenon to remain poorly understood, and contributes to the difficulty we face in predicting ligand–protein binding parameters.

**Received:** October 28, 2013
**Published:** January 30, 2014

   dx.doi.org/10.1021/jm401609a | *J. Med. Chem.* 2014, 57, 2315−2333

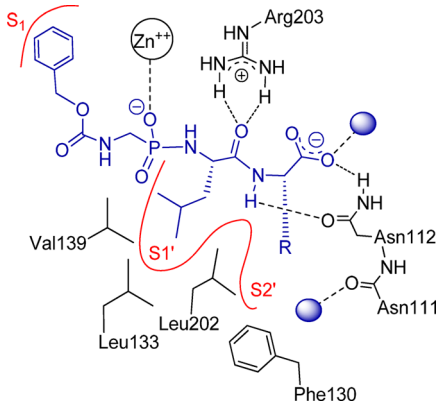


**Figure 1.** Thermolysin phosphonamidate inhibitors: The general scaffold is shown binding in the active site of thermolysin; R group represents different P2′ side chains binding in the shallow, flat, and solvent-exposed S2′ pocket. Other important features of the thermolysin active site shown are: the S1 and S1′ hydrophobic pockets, and the zinc ion which binds the O of phosphonamidate moiety.

An area that is largely unexplored in the field of studying the hydrophobic binding is the influence of neighboring groups on the thermodynamic signatures of hydrophobic associations (i.e., is the hydrophobic effect context dependent?). Studying neighboring group effects on hydrophobic interactions could refine our understanding of the hydrophobic effects and provide guidance for designing ligands that bind more tightly to proteins. Recently, the influence of the terminal carboxylate group of TLN phosphonamidate inhibitors on the contributions of the P2′ methyl side chain to the binding thermodynamic parameters was investigated.[16] In that study, the carboxylate group was found to favorably modulate the contributions of the Me group to both the enthalpy and the free energy of binding (positive cooperativity) and unfavorably modulate its contribution to the entropy of binding (negative cooperativity). These influences were attributed to variations in the thermodynamics of the changes caused by the Me group in the hydration status of the S2′ pocket when the Me group is incorporated in the ligand in the presence vs the absence of the nearby carboxylate group (Supporting Information: Figure S1). It is generally appreciated that the thermodynamic impact of the hydrophobic association of a particular ligand side chain with a protein pocket encompasses multiple effects such as the desolvation of the ligand side chain and the protein pocket, the dispersion interactions between the buried parts of the ligand side chain and the protein, and the resolvation of the unburied hydrophobic portion of the ligand−protein complex. However, the influence of neighboring groups on these effects is not usually considered. We herein hypothesize, upon the basis of our previously referred study,[16] that the influence of neighboring groups on these effects could be a general phenomenon that alters the thermodynamic signature of the hydrophobic binding of ligand side chains.

To probe this hypothesis further, isothermal titration calorimetry (ITC) was used to carry out an in-depth analysis of the incremental changes in the binding thermodynamic parameters ($\Delta\Delta G$, $\Delta\Delta H$, and $-T\Delta\Delta S$) associated with increasing both the size and the degree of branching of the P2′ side chain of the TLN phosphonamidate inhibitors. Two series of inhibitors were therefore designed: one with the terminal $COO^-$ group, which include the previously reported ligands[15] as well as ligands with longer (*n*-Bu) and more branched (*tert*-Bu and neopentyl) P2′ side chains (series "A"), and the other (series "B") lacking the terminal carboxylate but having the same P2′ side chains as those of series "A" ligands (Scheme 1). In the following sections, data obtained from ITC experiments are presented and discussed in relation to the above hypothesis.

**Scheme 1. Two Series of TLN Phosphonamidate Inhibitors: Series A Which Includes Ligands 1a−12a (with $COO^-$), and Series B Which Includes Ligands 1b−12b (without $COO^-$)[a]**

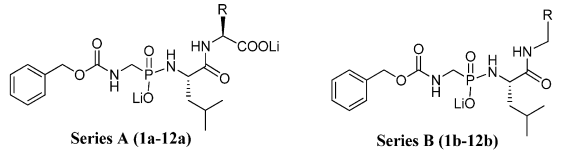


R = H (1a, 1b); $CH_3$ (2a, 2b); $CH_2CH_3$ (3a, 3b); $(CH_2)_2CH_3$ (4a, 4b); $(CH_2)_3CH_3$ (5a, 5b); $CH(CH_3)_2$ (6a, 6b); $C(CH_3)_3$ (7a, 7b); $CH(CH_3)CH_2CH_3$ (8a, 8b); $CH_2CH(CH_3)_2$ (9a, 9b); $CH_2C(CH_3)_3$ (10a, 10b); $CH_2C_6H_5$ (11a, 11b); and $CH_2C_4H_3S$ (12a, 12b).

[a]The R/P2′ side chains and the corresponding ligands are shown.

## RESULTS AND DISCUSSION

**Synthesis of the Ligands.** Ligands were synthesized according to the general protocol used for the previously reported TLN inhibitors (i.e., **1−2a** and **1−2b**).[16] First, the commercially available benzyl carbamate was heated in an aqueous basic formaldehyde solution to give benzyl *N*-(hydroxymethyl)carbamate **1**. The terminal hydroxyl group of intermediate **1** was acetylated using acetic anhydride to give benzyl *N*-(acetoxymethyl)carbamate **2**. Intermediate **2** was converted to dimethyl *N*-(benzyloxycarbonyl)-aminomethylphosphonate **3** by refluxing with trimethyl phosphite. Intermediate **4** was obtained by the hydrolysis of one of the two methyl phosphonate esters in **3** using 10% NaOH solution (Scheme 2).

**Scheme 2. Synthesis of Intermediate 4[a]**

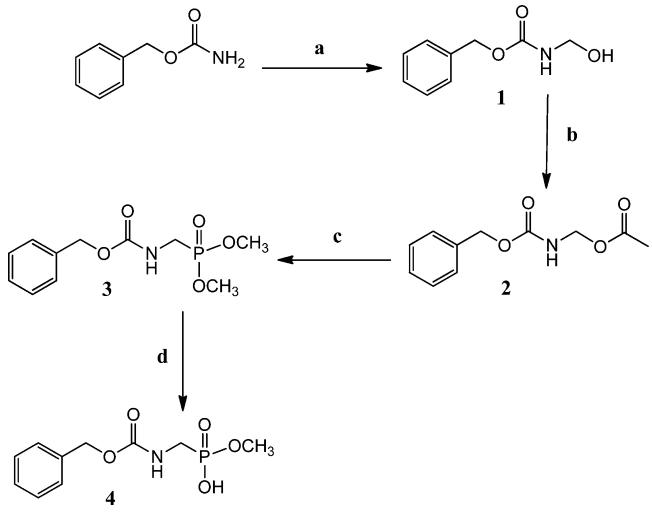


[a]Reagents and conditions: (a) 0.5 equiv of $Na_2CO_3$, 1.5 equiv of 37% HCHO, $H_2O$, rt, overnight, 74%; (b) excess $Ac_2O$, 6.0 equiv of pyridine, THF, rt, 2 h, 67%; (c) 3.0−4.0 equiv of $P(OCH_3)_3$, reflux, 3 h, 97%; (d) 6 equiv of 10% NaOH, rt, 2 h, 73%.


dx.doi.org/10.1021/jm401609a | J. Med. Chem. 2014, 57, 2315−2333

The synthesis of ligands **1a−12a** and **1a−12b** is shown in Scheme 3. As illustrated in this scheme, the commercially

**Scheme 3. Synthesis of Ligands 1a−12a and 1a−12b**[a]

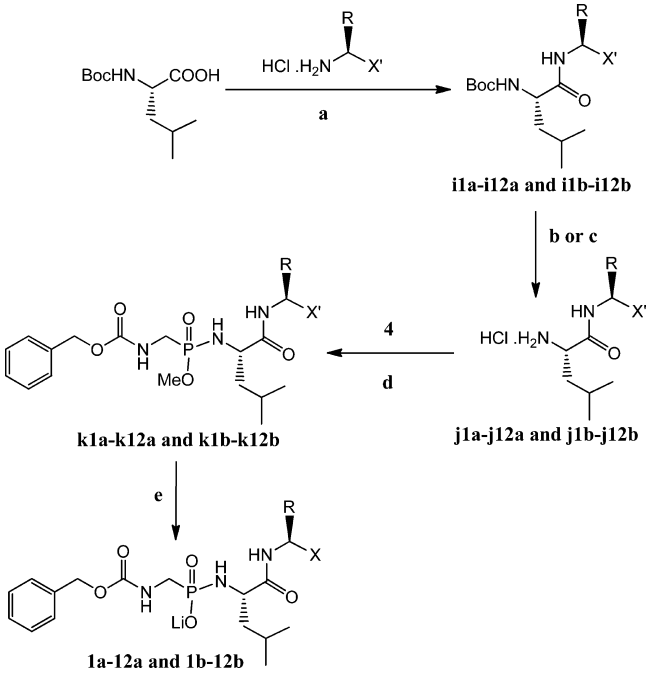


[a]Reagents and conditions: (a) 1.2 equiv of PyBop (or 1.2 equiv of EDCI·HCl, 1.2 equiv of HOBt), 3.3−4.0 equiv of DIEA, anhydrous DMF, rt, 5 h−overnight, 65−85%; (b) 3 M HCl/MeOH, rt, 2−3 h, 93−99%; (c) HCl gas, EtOAc, rt, 2−3 h, 97%; (d) 1.2 equiv of PyBop, 4.0 equiv of DIEA, anhydrous DCM, rt, 6 h−overnight, 45−75%; (e) 2.0−4.0 equiv of LiOH, $H_2O$/MeCN, rt, 2 h−overnight, 60−95%.

available Boc-Leu-OH was coupled to the hydrochloride salts of various amines or $\alpha$-amino esters to give the intermediates **i1a−i12a** and **i1b−i12b**. Either EDCI/HOBt or PyBop in anhydrous DMF was used effectively to achieve the coupling in the presence of diisopropylethylamine. The intermediates **j1a−j12a** and **j1b−j12b** were then obtained as hydrochloride salts upon the removal of the Boc groups from **i1a−i12a** and **i1b−i12b**. To remove the Boc groups, either 3 M HCl/MeOH solution was used or HCl gas was bubbled into an ethyl acetate solution of the Boc-protected intermediate to avoid transesterification with MeOH.

Finally, intermediate **4** was coupled to each of the intermediates **j1a−j12a** and **j1b−j12b** in anhydrous dichloromethane using PyBop as the coupling reagent to give **k1a−k12a** and **k1b−k12b**. Compounds **k1a−k12a** and **k1b−k12b** were then hydrolyzed using lithium hydroxide to give the final compounds **1a−12a** and **1a−12b** either as dilithium salts (when the carboxylate group is present) or monolithium salts (when the carboxylate group is absent). All the final compounds were purified by reverse-phase HPLC to at least 95% purity. The substitution pattern of the synthesized ligands and their intermediates is given in Table 1.

**Isothermal Titration Calorimetry (ITC).** ITC is the most widely used technology for measuring the thermodynamic parameters of ligand−protein binding.[17−20] One of the advantages of ITC is that all the binding parameters can be simultaneously determined in a single experiment at a fixed temperature. For example, both the enthalpy ($\Delta H$), the

**Table 1. Substitution Pattern of 1a−12a and 1a−12b and Their Intermediates**

| compounds | R | X′, X |
|---|---|---|
| **i1a, j1a, k1a, 1a** | H | COOEt, COOLi |
| **i2a, j2a, k2a, 2a** | Me | COOMe, COOLi |
| **i3a, j3a, k3a, 3a** | Et | COOMe, COOLi |
| **i4a, j4a, k4a, 4a** | *n*-Pr | COOMe, COOLi |
| **i5a, j5a, k5a, 5a** | *n*-Bu | COOMe, COOLi |
| **i6a, j6a, k6a, 6a** | *i*-Pr | COOMe, COOLi |
| **i7a, j7a, k7a, 7a** | *tert*-Bu | COOMe, COOLi |
| **i8a, j8a, k8a, 8a** | *sec*-Bu | COOMe, COOLi |
| **i9a, j9a, k9a, 9a** | *i*-Bu | COOMe, COOLi |
| **i10a, j10a, k10a, 10a** | neopentyl | COOMe, COOLi |
| **i11a, j11a, k11a, 11a** | Bn | COOMe, COOLi |
| **i12a, j12a, k12a, 12a** | 2-thienylmethyl | COOMe, COOLi |
| **i1b, j1b, k1b, 1b** | H | H, H |
| **i2b, j2b, k2b, 2b** | Me | H, H |
| **i3b, j3b, k3b, 3b** | Et | H, H |
| **i4b, j4b, k4b, 4b** | *n*-Pr | H, H |
| **i5b, j5b, k5b, 5b** | *n*-Bu | H, H |
| **i6b, j6b, k6b, 6b** | *i*-Pr | H, H |
| **i7b, j7b, k7b, 7b** | *tert*-Bu | H, H |
| **i8b, j8b, k8b, 8b** | *sec*-Bu | H, H |
| **i9b, j9b, k9b, 9b** | *i*-Bu | H, H |
| **i10b, j10b, k10b, 10b** | neopentyl | H, H |
| **i11b, j11b, k11b, 11b** | Bn | H, H |
| **i12b, j12b, k12b, 12b** | 2-thienylmethyl | H, H |

association constant ($K_a$), and the reaction stoichiometry ($n$) can be directly determined in an ITC experiment, and then the enthalpy and the association constant can be used to calculate both the binding free energy ($\Delta G$) and the entropic contribution to the binding process ($-T\Delta S$). Although the commercially available ITC instruments can produce data with approximately 1% relative standard error for $\Delta H$, $K_a$, and $n$, this error is largely underestimated.[21] One of the major sources of inaccuracies in ITC data is the uncertainty in the ligand and the protein concentrations. Protein concentration errors undermine the accuracy of the reaction stoichiometry ($n$), but, fortunately, they do not influence the accuracy of the other parameters. On the other hand, uncertainty in ligand concentration can cause large errors in the three parameters directly measured by the instrument ($\Delta H$, $K_a$, and $n$). For example, the interlaboratory variations in determining $\Delta H$ of the binding of 4-carboxybenzenesulfonamide (CBS) to bovine carbonic anhydrase II (CAII) was found to be ≈24% and was attributed to uncertainty in ligand concentration.[22] Failure to accurately determine the ligand concentration can cause apparent enthalpy−entropy compensation in ITC results that could be falsely attributed to a physical origin.[23] It was therefore crucial to the current study to address this issue in our experimental design in order to obtain valid conclusions with regard to the incremental changes in the enthalpy, entropy and free energy ($\Delta\Delta H$, $-T\Delta\Delta S$, and $\Delta\Delta G$). Details about the experimental design and the measures taken to address errors in ligand concentrations, as well as other experimental details, are provided in Supporting Information.

The thermodynamic data obtained for the 24 ligands tested in this study are given in Table S1 of the Supporting Information file. It should be noted that the binding of phosphonamidate inhibitors to TLN is accompanied by a protonation event (i.e., the ligand−protein complex picks up a


dx.doi.org/10.1021/jm401609a | J. Med. Chem. 2014, 57, 2315−2333

**Table 2. Differential (relative) Thermodynamic Data Caused by the Homologation of the R Side Chain in the Presence and Absence of the Neighboring $COO^-$ Group**

| hydrophobic modification | presence of $COO^-$ (kJ/mol) | | | absence of $COO^-$ (kJ/mol) | | |
|---|---|---|---|---|---|---|
| H→Me | $\Delta\Delta H_{1a\rightarrow2a} = -5.6$ | $-T\Delta\Delta S_{1a\rightarrow2a} = +0.5$ | $\Delta\Delta G_{1a\rightarrow2a} = -5.1$ | $\Delta\Delta H_{1b\rightarrow2b} = +1.6$ | $-T\Delta\Delta S_{1b\rightarrow2b} = -3.3$ | $\Delta\Delta G_{1b\rightarrow2b} = -1.7$ |
| Me→Et | $\Delta\Delta H_{2a\rightarrow3a} = -3.5$ | $-T\Delta\Delta S_{2a\rightarrow3a} = +3.2$ | $\Delta\Delta G_{2a\rightarrow3a} = -0.3$ | $\Delta\Delta H_{2b\rightarrow3b} = -6.5$ | $-T\Delta\Delta S_{2b\rightarrow3b} = +2.9$ | $\Delta\Delta G_{2b\rightarrow3b} = -3.6$ |
| Et→*n*-Pr | $\Delta\Delta H_{3a\rightarrow4a} = +4.8$ | $-T\Delta\Delta S_{3a\rightarrow4a} = -5.6$ | $\Delta\Delta G_{3a\rightarrow4a} = -0.8$ | $\Delta\Delta H_{3b\rightarrow4b} = +8.1$ | $-T\Delta\Delta S_{3b\rightarrow4b} = -7.4$ | $\Delta\Delta G_{3b\rightarrow4b} = +0.7$ |
| Et→*n*-Bu | $\Delta\Delta H_{3a\rightarrow5a} = +2.9$ | $-T\Delta\Delta S_{3a\rightarrow5a} = -3.3$ | $\Delta\Delta G_{3a\rightarrow5a} = -0.4$ | $\Delta\Delta H_{3b\rightarrow4b} = +7.8$ | $-T\Delta\Delta S_{3b\rightarrow5b} = -7.1$ | $\Delta\Delta G_{3b\rightarrow4b} = +0.7$ |

proton).[11,15] The enthalpy ($\Delta H_{obs}$) and the entropy ($-T\Delta S_{obs}$) values obtained in the ITC experiments (Table S1, Supporting Information), therefore, include significant contributions from the ionization of the HEPES buffer used in the experiments and are, consequently, not identical to the binding enthalpy and entropy ($\Delta H_{bind}$ and $-T\Delta S_{bind}$). However, $\Delta\Delta H_{obs}$ and $-T\Delta\Delta S_{obs}$ are equivalent to $\Delta\Delta H_{bind}$ and $-T\Delta\Delta S_{bind}$, because the same number of protons is picked up upon the binding of each ligand to the protein (the buffer ionization contributions are, consequently, equivalent and cancel out each other when a relative parameter such as $\Delta\Delta H_{obs}$ is determined).[15] Having mentioned this, it would be possible to use $\Delta\Delta H_{obs}$ and $-T\Delta\Delta S_{obs}$ for analyzing the incremental changes in the binding thermodynamic parameters across ligand series. In addition to this, a second potential contribution to the observed thermodynamic data might be caused by the displacement of the Val-Lys dipeptide, which is produced by the autoproteolysis of TLN at the high concentration used in ITC experiment, from the enzyme active site by the phosphonamidate ligands. This contribution is also expected to be the same for all ligands and therefore cancels out from the incremental changes in the thermodynamic parameters.[11,15]

In the following discussions, the ligands tested are grouped according to the type of modification made in the S2′-binding R side chains into

(1) ligands in which the R side chain is homologated in a linear fashion (**1a**−**5a** and **1b**−**5b**);
(2) ligands in which the R side chain is branched from either the $\beta$- (**3a**→**6a**→**7a** and **3b**→**6b**→**7b**; Also **4a**→**8a** and **4b**→**8b**) or the $\gamma$-C (**4a**→**9a**→**10a** and **4b**→**9b**→**10b**);
(3) ligands in which an aromatic moiety (phenyl, thienyl) replaces one of H atoms of the methyl side chain (**2a**→**11a**/**12a** and **2b**→**11b**/**12b**).

The relative/differential thermodynamic profiles within each of these groups, as well as the influence of the neighboring $COO^-$ group on these thermodynamic profiles, were investigated and correlated with the aforementioned hydrophobic modifications. It should be noted that differential thermodynamic profiles were previously factorized into elementary components based on thermodynamic cycles which involve mutating one ligand to another both in the unbound and the complexed states.[16] Such factorization is illustrated by the master eqs 1A−1C whose mathematical terms correspond to the physical changes occurring in the unbound ligand and the ligand−protein complex systems when the ligand structure is modified. In the current study, these master equations were frequently employed to qualify or disqualify these physical changes as potential causes for the experimentally observed differential thermodynamic profile and the influence of the $COO^-$ on these profiles.

$$\begin{aligned}\Delta\Delta G_{(R\rightarrow R')} &= \Delta G_{b\text{-}solv} + \Delta G_{b\text{-}R'/R} \\ &\quad - (\Delta G_{a\text{-}solv} + \Delta G_{a\text{-}R'/R}) \\ &= \Delta G_{b\text{-}Wdisp} + \Delta G_{b\text{-}Wstrct} + \Delta G_{b\text{-}R'/R} \\ &\quad - (\Delta G_{a\text{-}solv} + \Delta G_{a\text{-}R'/R}) \end{aligned} \quad (1A)$$

$$\begin{aligned}\Delta\Delta H_{(R\rightarrow R')} &= \Delta H_{b\text{-}solv} + \Delta H_{b\text{-}R'/R} \\ &\quad - (\Delta H_{a\text{-}solv} + \Delta H_{a\text{-}R'/R}) \\ &= \Delta H_{b\text{-}Wdisp} + \Delta H_{b\text{-}Wstrct} + \Delta H_{b\text{-}R'/R} \\ &\quad - (\Delta H_{a\text{-}solv} + \Delta H_{a\text{-}R'/R}) \end{aligned} \quad (1B)$$

$$\begin{aligned}-T\Delta\Delta S_{(R\rightarrow R')} &= -T\Delta S_{b\text{-}solv} + (-T\Delta S_{b\text{-}R'/R}) \\ &\quad - (-T\Delta S_{a\text{-}solv} + (-T\Delta S_{a\text{-}R'/R})) \\ &= -T\Delta S_{b\text{-}Wdisp} + (-T\Delta S_{b\text{-}Wstrct}) \\ &\quad + (-T\Delta S_{b\text{-}R'/R}) \\ &\quad - (-T\Delta S_{a\text{-}solv} + (-T\Delta S_{a\text{-}R'/R})) \end{aligned} \quad (1C)$$

According to eqs 1A−1C, the differential thermodynamic parameters are contributed by

(1) changes in the hydration layer of the ligand−protein complex that occur upon modifying the ligand structure (terms with the subscript "b-solv");
(2) the gain, loss, strengthening, and/or weakening of noncovalent interactions (e.g., H-bonds, dispersion interactions, etc.) in the ligand−protein system; as well as the conformational entropy changes caused by ligand modification/functional group replacement (terms with the subscript "b-R′/R″ for the R→R′ replacement);
(3) changes in the hydration status of the unbound ligand (terms with the subscript "a-solv");
(4) changes in both the noncovalent interactions and the conformational entropy of the unbound hydrated ligand (terms with the subscript "a-R′/R″).

The contribution of the first category can be further dissected into a contribution from the displacement of water from the ligand−protein complex (terms with the subscript "b-Wdisp") and a contribution from the incorporation of new waters in the crystallographic water set of the complex (terms with the subscript "b-Wstrct"). Changes in the hydration layer of the ligand−protein complex can be studied using high resolution X-ray crystallography. For example, both the water displacement and the water acquisition can be identified when the crystal structures of the unmodified and the modified ligands are superimposed. The waters in the structure of the former ligand that are missing from the structure of the latter are considered to be displaced, and those in the latter but not in the former are considered to be acquired from the bulk solvent upon carrying


dx.doi.org/10.1021/jm401609a | J. Med. Chem. 2014, 57, 2315−2333

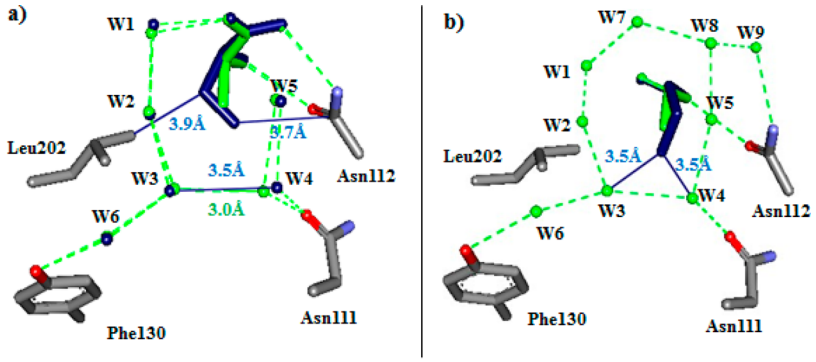


**Figure 2.** (a) Superimposition of the crystal structures of the **3a**−TLN and the **2a**−TLN complexes. Ligand **3a** and water molecules that belong to its complex are shown in blue. Ligand **2a** and water molecules that belong to its complex are shown in green. Minimal changes in hydration layer, the most significant of which is the elongation of the H-bond between W3 and W4, are observed. Ligand **3a** has additional contacts with both Leu202 and Asn112 (distances are shown). (b) Superimposition of the minimized structure of **3b** on the crystal structure of the **2b**−TLN complex. Ligand **3b** is shown in blue. Ligand **2b** and water molecules that belong to its complex are shown in green. Ligand **3b** has mild steric clashes with W3 and W4 (indicated by the relatively short distances between the ligand side chain and these waters). In both a and b, protein atoms are shown in the following colors: C (gray), O (red), and N (blue). Some water molecules and protein residues are not shown for clarity.

out the ligand modification. Such superimposition technique is often employed herein. It should be noted, however, that crystallographic waters are the least reliable component of a crystal structure. While X-ray crystallography is a better technique than, for example, calculations to determine the positions of water molecules in the ligand−protein complex, interpretations based upon crystallographic waters' data should not be viewed as impregnable. These interpretations might be challenged if experimental techniques that provide more reliable information about crystallographic waters become available and are used to tackle such a complex problem.

*1. Side-Chain Homologation.* Table 2 lists the differential thermodynamic data produced by homologating the R side chain in the presence and absence of the neighboring $COO^-$ group. Going from H to Me in the presence of the $COO^-$ group (**1a**→**2a**) causes an improvement in both the binding enthalpy and the binding free energy (Table 2: $\Delta\Delta H_{1a\rightarrow 2a}$ = −5.6 kJ/mol, $\Delta\Delta G_{1a\rightarrow 2a}$ = −5.1 kJ/mol). On the other hand, in the absence of the $COO^-$ (**1b**→**2b**), some improvement in both the entropy and the free energy ($-T\Delta\Delta S_{1b\rightarrow 2b}$ = −3.3 kJ/mol, $\Delta\Delta G_{1b\rightarrow 2b}$ = −1.7 kJ/mol), as well as a slight worsening in the enthalpy ($\Delta\Delta H_{1b\rightarrow 2b}$ = 1.6 kJ/mol), occurs. Crystallographic data of ligands **1**−**2a** and **1**−**2b** previously revealed that the replacement of the H atoms in **1a** and **1b** with Me groups in the bound state is accompanied by (1) displacement of crystallographic waters from the ligand−protein complex ($\Delta H_{b\text{-}Wdisp} > 0$ and $-T\Delta S_{b\text{-}Wdisp} < 0$; contributes unfavorably to $\Delta\Delta H_{(H\rightarrow Me)}$ and favorably to $-T\Delta\Delta S_{(H\rightarrow Me)}$); and (2) incorporation of new crystallographic waters in positions of the complex hydration layer different from the positions of the displaced waters ($\Delta H_{b\text{-}Wstrct} < 0$ and $-T\Delta S_{b\text{-}Wstrct} > 0$; contributes favorably to $\Delta\Delta H_{(H\rightarrow Me)}$ and unfavorably to $-T\Delta\Delta S_{(H\rightarrow Me)}$).[16] In the unbound state, the H→Me replacement potentially causes the hydration waters to become more organized around the Me side chain ($-T\Delta S_{a\text{-}solv} > 0$; contributes favorably to $-T\Delta\Delta S_{(H\rightarrow Me)}$: classic hydrophobic effect). Using eqs 1B and 1C, it could be concluded that the −5.6 kJ/mol differential enthalpy caused by the replacement of the H in **1a** with Me is most likely attributed to $\Delta H_{b\text{-}Wstrct}$ dominating other enthalpic components, and the −3.3 kJ/mol differential entropy caused by the replacement of the H in **1b** with Me is most likely attributed to $-T\Delta S_{b\text{-}Wdisp}$ and $-T\Delta S_{a\text{-}solv}$ dominating other entropic components.

Furthermore, crystallographic and quantum mechanical data[16] suggested that the improvement of $\Delta\Delta H_{(H\rightarrow Me)}$ caused by the $COO^-$ ($\Delta\Delta H_{1a\rightarrow 2a} - \Delta\Delta H_{1b\rightarrow 2b}$ = −7.2 kJ/mol) can be attributed to (1) a smaller enthalpic penalty for displacing water molecules that are less tightly bound in the complex of **1a** than in the complex of **1b** (↓ $\Delta H_{b\text{-}Wdisp}$); and (2) a greater enthalpic advantage for acquiring a larger number of crystallographic waters and forming a more coherent water network in the complex of **2a** (↓ $\Delta H_{b\text{-}Wstrct}$). The worsening of $-T\Delta\Delta S_{(H\rightarrow Me)}$) in the presence of the $COO^-$ [$-T\Delta\Delta S_{1a\rightarrow 2a} - (-T\Delta\Delta S_{1b\rightarrow 2b})$ = 3.8 kJ/mol] could be viewed as a result of enthalpy−entropy compensation effects in both the water displacement and the water acquisition contributions.

*1.1. Me→Et (a favorable ΔΔH opposed by the $COO^-$).* The replacement of Me with Et in the presence of the $COO^-$ group (**2a**→**3a**) causes some additional improvement in the enthalpy of binding (Table 2: $\Delta\Delta H_{2a\rightarrow 3a}$ = −3.5 kJ/mol). This enthalpic improvement is compensated by an entropic penalty which almost cancels any advantageous effect on the binding affinity ($-T\Delta\Delta S_{2a\rightarrow 3a}$ = 3.2 kJ/mol, $\Delta\Delta G_{2a\rightarrow 3a}$ = −0.3 kJ/mol). Crystallographic data of the complexes of **2a** and **3a** with TLN reveal that when the Me of **2a** is replaced with Et, minimal changes in the hydration layer of the ligand−protein complex take place.[24] The most significant of these changes is the elongation, and probably the weakening, of the H-bond between W3 and W4 (Figure 2a). These crystallographic findings can be translated into insignificant $\Delta H_{b\text{-}solv}$ and $-T\Delta S_{b\text{-}solv}$ values, which would not contribute much to the differential thermodynamic parameters (i.e., $\Delta\Delta H_{2a\rightarrow 3a}$ and $-T\Delta\Delta S_{2a\rightarrow 3a}$). It should be noted that even if the elongation and any associated reduction in the strength of the aforementioned H-bond would be considered significant, the hydration layer changes would contribute in the opposite direction to the observed differential enthalpy and entropy. This is because $\Delta H_{b\text{-}solv}$ would be positive and consequently contribute unfavorably to $\Delta\Delta H_{(Me\rightarrow Et)}$, and $-T\Delta S_{b\text{-}solv}$ would be negative and consequently contribute favorably to $-T\Delta\Delta S_{(Me\rightarrow Et)}$ (eqs 1B and 1C). It can therefore be concluded that, unlike the **1a**→**2a** transition, the enthalpic improvement and the entropic penalty associated with the **2a**→**3a** transition


dx.doi.org/10.1021/jm401609a | J. Med. Chem. 2014, 57, 2315−2333

cannot be attributed to any significant change in the hydration pattern of the S2′ pocket region.

The enthalpic advantage could be contributed by some additional dispersion forces between the Et side chain (vs the Me) and the protein (Figure 2a: $\Delta H_{\text{b-Et/Me}} < 0$), but more importantly, it could be contributed by a decreased ability of the hydration waters in the unbound state to maintain a highly organized cluster, with reinforced H-bonds, around the Et side chain ($\Delta H_{\text{a-solv}} > 0$; contributes favorably to $\Delta\Delta H_{(\text{Me}\rightarrow\text{Et})}$; eq 1B). It was previously pointed out that the thermodynamic signature of the hydrophobic effect is dependent on the size of the nonpolar solute (the length scale dependency of hydrophobicity).[25−29] For example, a small hydrophobic solute does not interfere with the ability of the hydration waters to retain their full set of H-bonds but causes these hydration waters to restrict their motions in order to minimize the contact of their H-bonding arms with the hydrophobic surface. The hydration of small nonpolar solutes is therefore opposed by the entropic penalty of water organization, rather than by enthalpic penalty. On the other hand, as the solute size grows, it becomes more difficult for water molecules to fully retain their H-bonds, and consequently hydrophobic hydration becomes increasingly associated with the enthalpic penalty of breaking H-bonds. Previously, it has been shown that replacing the H in the unbound ligand with Me is not likely to interfere with the H-bonding of the interfacial waters because these waters could accommodate a small-sized side chain such as the Me.[16] Rather, the Me could reduce the mobility of these water molecules and produce an entropic penalty ($-T\Delta S_{\text{a-solv}} > 0$). Conversely, when the Me is grown to Et, the hydration waters most likely encounter geometrical challenges to maintain a relatively stable H-bond network, and as a consequence, the solvent disorganization/H-bond breaking effect emerges and produces a positive $\Delta H_{\text{a-solv}}$ and a negative $-T\Delta S_{\text{a-solv}}$ terms. Given that a negative $-T\Delta S_{\text{a-solv}}$ contributes unfavorably to $-T\Delta\Delta S_{(\text{Me}\rightarrow\text{Et})}$ (eq 1C), solvent disorganization could be responsible not only for the enthalpic advantage but also for the entropic penalty observed when the Me of **2a** is replaced with Et.

In the absence of the $COO^-$ group, the replacement of the Me group with Et (**2b**→**3b**) causes an enthalpic improvement which is greater in magnitude than that caused by the same replacement in the presence of the $COO^-$ (Table 2: $\Delta\Delta H_{\text{2b}\rightarrow\text{3b}} = -6.5$ kJ/mol). On the other hand, **2b**→**3b** causes an entropic penalty of similar magnitude to that produced by the **2a**→**3a** transition ($-T\Delta\Delta S_{\text{2b}\rightarrow\text{3b}} = 2.9$ kJ/mol). The binding free energy, consequently, is improved by 3.6 kJ/mol ($\Delta\Delta G_{\text{2b}\rightarrow\text{3b}} = -3.6$ kJ/mol). Putting it differently, the $COO^-$ group opposes both the favorable differential enthalpy and the favorable differential free energy (Figure 3). This trend is the opposite of what was observed with the H→Me replacement, wherein the $COO^-$ improves both of these differential parameters [Note: when "improved differential enthalpy" is mentioned, we mean that the quantity $\Delta\Delta H$, whether it is positive or negative, shifts to the negative, but when "improved enthalpy" is mentioned, we mean that $\Delta\Delta H$ itself is negative ($\Delta H$ is the quantity that shifts to the negative)—the same applies to other thermodynamic quantities]. To explain these data, the individual components of differential thermodynamic parameters need to be investigated in light of the following questions:

*Can the Hydration Status Changes of the Ligand−Protein Complex Be Responsible for the Improved Differential Enthalpy Caused by the Absence of the $COO^-$?* To answer this question, the ligand Me side chain in the crystal structure

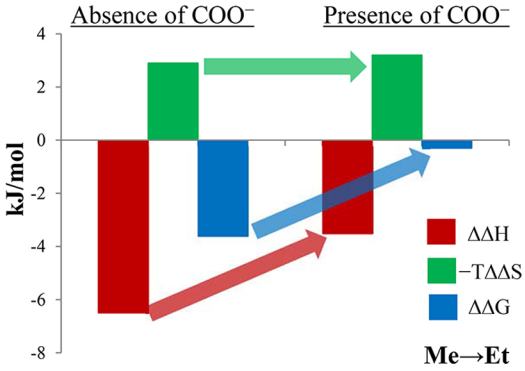


**Figure 3.** The differential thermodynamic parameters of the hydrophobic modification Me→Et, in the absence and presence of the neighboring $COO^-$ group. $\Delta\Delta H$ is red, $-T\Delta\Delta S$ is green, and $\Delta\Delta G$ is blue. A negative differential thermodynamic parameter indicates that the hydrophobic modification in question (i.e., Me→Et) is favorable with regard to this parameter and vice versa. An arrow indicates how the $COO^-$ influences a differential thermodynamic parameter. An arrow going up illustrates a shift toward a more positive (unfavorable) value and vice versa.

of the **2b**−TLN complex was grown to an Et in silico (e.g., to give ligand **3b**). This Et side chain was built in a number of conformations, each of which was minimized after removing all of the hydration waters from the complex, adding the missing hydrogen atoms, and constraining all of the remaining ligand and protein heavy atoms. The minimized structures were then superimposed on the original crystal structure of the **2b**−TLN complex, in order to investigate whether the Et side chain is compatible with the crystallographic waters of this complex or not. One of the modeled Et conformations was found to be sterically compatible with all of the water molecules in the S2′ region, except for mild steric clashes with two of the water molecules that constitute the heptagonal water structure hydrating the Me side chain of **2b** (i.e., W3 and W4, Figure 2b). These steric clashes, however, might not significantly disturb the heptagonal water structure because they can be relieved if these water molecules are slightly moved (e.g., W4 could be moved to a position similar to where it is in the **3a**−TLN complex). If the Et side chain predominantly adopts this conformation, the minimal changes in the S2′ pocket hydration pattern can be translated into insignificant $\Delta H_{\text{b-solv}}$ and $-T\Delta S_{\text{b-solv}}$ values—the first outcome.

In contrast, the other potential Et conformations in **3b** sterically interfere with some of the crystallographic waters of the heptagonal water structure (Supporting Information: Figure S2). If the Et side chain, consequently, adopts any of these conformations, water molecules are displaced from the complex causing $\Delta H_{\text{b-solv}}$ to be positive (due to the loss in H-bonding) and $-T\Delta S_{\text{b-solv}}$ to be negative (due to the increase in the mobility of the displaced waters when they move to the bulk solvent)—the second outcome. It is, however, unlikely for the Et to predominantly do so, because the heptagonal water structure is potentially one of the favorable components of the system in terms of free energy, and consequently the conformation that allows retaining this structure with minimal free energy cost would be preferred (i.e., the one shown in Figure 2b). Applying eqs 1B and 1C, it can be concluded that neither the first nor the second outcome explains the enthalpic advantage/entropic penalty observed when the Me is replaced with Et in the absence of the $COO^-$ group (considering the

first outcome, the insignificant $\Delta H_{\text{b-solv}}$ and $-T\Delta S_{\text{b-solv}}$ contribute insignificantly to $\Delta\Delta H_{(\text{Me}\rightarrow\text{Et})}$ and $-T\Delta\Delta S_{(\text{Me}\rightarrow\text{Et})}$; alternatively, the positive $\Delta H_{\text{b-solv}}$ and the negative $-T\Delta S_{\text{b-solv}}$ of the second outcome contribute unfavorably to $\Delta\Delta H_{(\text{Me}\rightarrow\text{Et})}$ and favorably to $-T\Delta\Delta S_{(\text{Me}\rightarrow\text{Et})}$, respectively).

This, however, does not necessarily mean that this factor is not responsible for the improved differential enthalpy/free energy caused by the absence of the $COO^-$ ($\Delta\Delta H_{\mathbf{2b}\rightarrow\mathbf{3b}} - \Delta\Delta H_{\mathbf{2a}\rightarrow\mathbf{3a}} = -3.0$ kJ/mol; $\Delta\Delta G_{\mathbf{2b}\rightarrow\mathbf{3b}} - \Delta\Delta G_{\mathbf{2a}\rightarrow\mathbf{3a}} = -3.3$ kJ/mol). To investigate this, we need to determine which of the hydration changes of the **2a**−TLN→**3a**−TLN and those of the **2b**−TLN→**3b**−TLN are more enthalpically advantageous. Depending on whether the first or the second of the previously mentioned outcomes is obtained when the Me is replaced with Et in the absence of the $COO^-$, the hydration changes of **2b**−TLN→**3b**−TLN would elicit either equal or larger enthalpic penalty than the hydration changes of **2a**−TLN→**3a**−TLN. In other words, the absence of the $COO^-$ either minimally influences or increases $\Delta H_{\text{b-solv}}$. This is, consequently, reflected as either minimal influence on or an increase in $\Delta\Delta H_{(\text{Me}\rightarrow\text{Et})}$, rather than a decrease in $\Delta\Delta H_{(\text{Me}\rightarrow\text{Et})}$ as we observe in the ITC data. It can therefore be concluded that the improved differential enthalpy/free energy caused by the absence of the $COO^-$ is not caused by the potential hydration status changes associated with the Me→Et transition in the ligand−protein complex.

*Can the Hydration Status Changes of the Unbound Ligand Be Responsible for the Improved Differential Enthalpy Caused by the Absence of the $COO^-$?* In the previous discussion, it was pointed out that the enthalpic improvement and the entropic penalty which are observed when the Me is replaced with Et in the presence of the $COO^-$ group (i.e., the negative $\Delta\Delta H_{(\text{Me}\rightarrow\text{Et})}$ and the positive $-T\Delta\Delta S_{(\text{Me}\rightarrow\text{Et})}$) are most likely caused by a decrease in the organization of the water molecules hydrating the Et side chain. In the absence of the $COO^-$, it would be anticipated that the same solvent effect occurs, but probably to a larger extent, because the $COO^-$ in ligand **3a** could still provide some degree of support, via charge-assisted H-bonding, to the water cluster hydrating the neighboring Et group (Figure 4). This support is not available in ligand **3b**, and the hydration waters of this ligand are therefore anticipated to be less ordered. This could be translated into that the presence of the $COO^-$ group, while the ligand side chain is grown from Me to Et, causes $\Delta H_{\text{a-solv}}$ to be less unfavorable ($\downarrow\Delta H_{\text{a-solv}}$) and $-T\Delta S_{\text{a-solv}}$ to be less favorable ($\uparrow -T\Delta S_{\text{a-solv}}$) than in the absence of this group.

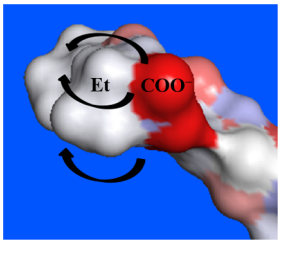


**Figure 4.** Ligand **3a** and its solvent-accessible surface colored according to atom partial charges (white: neutral; red: negatively charged; blue: positively charged). The ligand conformation shown is taken from the crystallographic complex of **3a** with TLN. The black arrows represent potential influences of the $COO^-$ group on the water molecules hydrating the Et group. These influences include H-bonding and electrostatic interactions.

Applying eq 1B, a decrease in $\Delta H_{\text{a-solv}}$ in the presence of the $COO^-$ shifts $\Delta\Delta H_{(\text{Me}\rightarrow\text{Et})}$ toward the positive, and this is what we observe in the ITC data (i.e., $\Delta\Delta H_{\mathbf{2a}\rightarrow\mathbf{3a}} = -3.5$ kJ/mol, while $\Delta\Delta H_{\mathbf{2b}\rightarrow\mathbf{3b}} = -6.5$ kJ/mol). Although the $COO^-$ group causes $-T\Delta S_{\text{a-solv}}$ to be less favorable and this supposedly shifts $-T\Delta\Delta S_{(\text{Me}\rightarrow\text{Et})}$ toward the negative, this shift is not experimentally observed (i.e., $-T\Delta\Delta S_{\mathbf{2a}\rightarrow\mathbf{3a}}$ and $-T\Delta\Delta S_{\mathbf{2b}\rightarrow\mathbf{3b}}$ are almost equal). The potential reasons for this are discussed in the supplementary figures and discussions in the Supporting Information. It should be noted that the $COO^-$ group is anticipated to affect $\Delta H_{\text{a-solv}}$ similarly in the case of the H→Me replacement.[16] This effect, however, is not translated into a positive shift in $\Delta\Delta H_{(\text{H}\rightarrow\text{Me})}$, like in the case of the Me→Et replacement. This is because the effect of the $COO^-$ on $\Delta H_{\text{a-solv}}$, in the case of the H→Me replacement, is overwhelmed by a larger effect on the enthalpic contribution of the changes occurring in the hydration layer of the ligand−protein complex, which influences the differential enthalpy in an opposite direction (i.e., the $COO^-$ $\downarrow\downarrow\Delta H_{\text{b-solv}}\rightarrow$ negative shift in $\Delta\Delta H_{(\text{H}\rightarrow\text{Me})}$).

*1.2. Et→n-Pr/n-Bu (an unfavorable $\Delta\Delta H$ and a favorable $-T\Delta\Delta S$ opposed by the $COO^-$).* Table 2 reveals that the replacement of the Et side chain with either *n*-Pr or *n*-Bu in the presence of the $COO^-$ group (**3a**→**4a** or **3a**→**5a**) is enthalpically unfavorable ($\Delta\Delta H_{\mathbf{3a}\rightarrow\mathbf{4a}} = 4.8$ kJ/mol and $\Delta\Delta H_{\mathbf{3a}\rightarrow\mathbf{5a}} = 2.9$ kJ/mol) and entropically favorable ($-T\Delta\Delta S_{\mathbf{3a}\rightarrow\mathbf{4a}} = -5.6$ kJ/mol and $-T\Delta\Delta S_{\mathbf{3a}\rightarrow\mathbf{5a}} = -3.3$ kJ/mol). The nearly complete compensation that is observed between the differential enthalpy and the differential entropy in both the Et→*n*-Pr and the Et→*n*-Bu replacements produces insignificant differential free energies ($\Delta\Delta G_{\mathbf{3a}\rightarrow\mathbf{4a}} = -0.8$ kJ/mol and $\Delta\Delta G_{\mathbf{3a}\rightarrow\mathbf{5a}} = -0.4$ kJ/mol). To explain these data, the crystal structures of the **4a**−TLN and the **3a**−TLN complexes were studied. These crystal structures revealed that some ordered water molecules which exist in the **3a**−TLN complex disappear from the **4a**−TLN complex. The disappearance of these water molecules could be explained either by water displacement from the complex hydration layer or by an increase in water mobility due to loss of H-bonding. The increased mobility of water molecules and the accompanying loss of H-bonding, whether occurring in the bulk solvent after displacement from the complex or within the complex hydration layer, could be thermodynamically translated into a negative $-T\Delta S_{\text{b-Wdisp}}$ and a positive $\Delta H_{\text{b-Wdisp}}$.

It is also noted that, going from Et to *n*-Pr, there is water gain as well, which can be translated into a positive $-T\Delta S_{\text{b-Wstrct}}$ term and a negative $\Delta H_{\text{b-Wstrct}}$ term. These terms are, however, not likely to overcome the negative $-T\Delta S_{\text{b-Wdisp}}$ and the positive $\Delta H_{\text{b-Wdisp}}$, because the new waters cannot regain the interconnected stable H-bond network that is lost upon the previously mentioned water displacement (a more detailed analysis of the crystallographic data is included in the supplementary discussions of the Supporting Information: Figure S3a). $\Delta H_{\text{b-solv}}$, which is the sum of $\Delta H_{\text{b-Wdisp}}$ and $\Delta H_{\text{b-Wstrct}}$, is therefore anticipated to be positive (a net decrease in H-bonding); and $-T\Delta S_{\text{b-solv}}$, which is the sum of $-T\Delta S_{\text{b-Wdisp}}$ and $-T\Delta S_{\text{b-Wstrct}}$, is anticipated to be negative (a net increase in water mobility). It should be noted that this trend is likely maintained and may even become more prominent (e.g., more waters could be displaced) when the Et is replaced by *n*-Bu. Using eqs 1B and 1C, it can be shown that the positive $\Delta H_{\text{b-solv}}$ contributes unfavorably to $\Delta\Delta H_{(\text{Et}\rightarrow n\text{-Pr}/n\text{-Bu})}$, and the negative $-T\Delta S_{\text{b-solv}}$ contributes


dx.doi.org/10.1021/jm401609a | J. Med. Chem. 2014, 57, 2315−2333

favorably to $-T\Delta\Delta S_{(Et\rightarrow n\text{-}Pr/n\text{-}Bu)}$. Because $\Delta\Delta H_{(Et\rightarrow n\text{-}Pr/n\text{-}Bu)}$ and $-T\Delta\Delta S_{(Et\rightarrow n\text{-}Pr/n\text{-}Bu)}$ were experimentally shown to be unfavorable and favorable, respectively, it can be concluded that, as the Et side chain grows larger, the changes in the hydration status of the S2′ pocket become responsible for the incremental thermodynamic changes observed in the ITC data.

Concerning the other enthalpic terms in eq 1B, neither $\Delta H_{b\text{-}R'/R}$ nor $\Delta H_{a\text{-}solv}$ are likely to be coresponsible for the unfavorable $\Delta\Delta H_{(Et\rightarrow n\text{-}Pr/n\text{-}Bu)}$. $\Delta H_{b\text{-}R'/R}$, for instance, is anticipated to be negative in both the Et→*n*-Pr and the Et→*n*-Bu replacements because of some additional dispersion interactions between the ligand and the protein. This term, consequently, contributes favorably to $\Delta\Delta H_{(Et\rightarrow n\text{-}Pr/n\text{-}Bu)}$. With regard to $\Delta H_{a\text{-}solv}$, it was previously mentioned that some degree of water organization could be maintained in ligand **3a** due to the presence of the $COO^-$ group. This residual water organization might gradually decrease when the size of the side chain increases from Et to *n*-Pr and then to *n*-Bu, even when the $COO^-$ still exists (e.g., the $COO^-$ becomes less capable of opposing the increasing geometrical challenges imposed on the water network by larger side chains). $\Delta H_{a\text{-}solv}$ could therefore be positive, and consequently, as with $\Delta H_{b\text{-}R'/R}$, this term could contribute favorably to $\Delta\Delta H_{(Et\rightarrow n\text{-}Pr/n\text{-}Bu)}$. $\Delta H_{b\text{-}R'/R}$ and $\Delta H_{a\text{-}solv}$ could however be responsible for the less unfavorable differential enthalpy of the Et→*n*-Bu replacement (2.9 vs 4.8 kJ/mol in the Et→*n*-Pr replacement). This is because the "*n*-Bu" side chain is anticipated to have more contacts with the protein than the "*n*-Pr", and consequently $\Delta H_{b\text{-}n\text{Bu/Et}}$ could be more negative than $\Delta H_{b\text{-}n\text{Pr/Et}}$ and contributes more favorably to $\Delta\Delta H_{(Et\rightarrow n\text{-}Bu)}$ than $\Delta H_{b\text{-}n\text{Pr/Et}}$ does to $\Delta\Delta H_{(Et\rightarrow n\text{-}Pr)}$. Also, the hydration waters are anticipated to be less ordered and to experience less H-bonding in the case of the "*n*-Bu" side chain, causing $\Delta H_{a\text{-}solv}$ to be more positive and to contribute more favorably to the differential enthalpy.

This solvent disorganization could also explain the less favorable differential entropy of the Et→*n*-Bu replacement (−3.3 vs −5.6 kJ/mol in the Et→*n*-Pr replacement), because the less ordered hydration waters in the case of the "*n*-Bu" side chain would be anticipated to cause $-T\Delta S_{a\text{-}solv}$ to be more negative and to contribute more unfavorably to the differential entropy (eq 1C). Although the trend in $-T\Delta S_{a\text{-}solv}$ could explain the variation in the differential entropy of the Et→*n*-Bu vs the Et→*n*-Pr replacement, $-T\Delta S_{a\text{-}solv}$ cannot be coresponsible with $-T\Delta S_{b\text{-}solv}$ for the favorable $-T\Delta\Delta S_{(Et\rightarrow n\text{-}Pr/n\text{-}Bu)}$ observed experimentally. This is because the anticipated negative $-T\Delta S_{a\text{-}solv}$ caused by solvent disorganization contributes unfavorably, rather than favorably, to $-T\Delta\Delta S_{(Et\rightarrow n\text{-}Pr/n\text{-}Bu)}$. Likewise, $-T\Delta S_{a\text{-}R'/R}$ cannot be coresponsible for the favorable $-T\Delta\Delta S_{(Et\rightarrow n\text{-}Pr/n\text{-}Bu)}$. This term is anticipated to be negative because of the increase in the conformational entropy caused by the additional rotatable bonds in the "*n*-Pr" and the "*n*-Bu" side chains, and therefore contributes unfavorably to $-T\Delta\Delta S_{(Et\rightarrow n\text{-}Pr/n\text{-}Bu)}$.

In the absence of the $COO^-$ group, the replacement of the Et side chain with either *n*-Pr or *n*-Bu (**3b**→**4b** or **3b**→**5b**) causes enthalpic penalty and entropic improvement that are larger than those occurring when the same side chain replacement is carried out in the presence of the $COO^-$ group (i.e., $\Delta\Delta H_{3b\rightarrow 4b}$ = 8.1 kJ/mol, $-T\Delta\Delta S_{3b\rightarrow 4b}$ = −7.4 kJ/mol, $\Delta\Delta H_{3b\rightarrow 5b}$ = 7.8 kJ/mol, and $-T\Delta\Delta S_{3b\rightarrow 5b}$ = −7.1 kJ/mol; Table 2). Like in the presence of the $COO^-$, no significant change in the binding free energy occurs ($\Delta\Delta G_{3b\rightarrow 4b}$ = 0.7 kJ/mol and $\Delta\Delta G_{3b\rightarrow 5b}$ = 0.7 kJ/mol). The $COO^-$ group, therefore, mitigates the enthalpic penalty and limits the entropic improvement of the Et→*n*-Pr/*n*-Bu replacement (in other words, it shifts $\Delta\Delta H$ toward the negative and $-T\Delta\Delta S$ toward the positive: Figure 5).

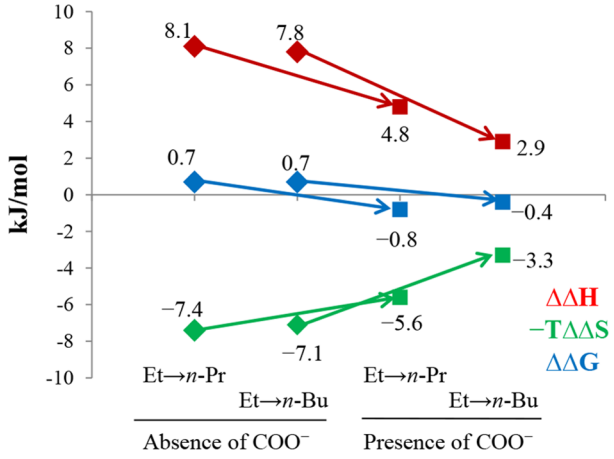


**Figure 5.** The differential thermodynamic parameters of the hydrophobic modifications Et→*n*-Pr and Et→*n*-Bu, in the absence and presence of the neighboring $COO^-$ group. $\Delta\Delta H$ is red, $-T\Delta\Delta S$ is green, and $\Delta\Delta G$ is blue. A negative differential thermodynamic parameter indicates that the hydrophobic modification in question is favorable with regard to this parameter and vice versa. An arrow indicates how the $COO^-$ influences a differential thermodynamic parameter. An arrow going up illustrates a shift toward a more positive (unfavorable) value and vice versa.

Considering some of the potential binding modes of the *n*-Pr side chain in the S2′ pocket, which are predicted by molecular modeling, in relation to the crystallographic waters of the **2b**–TLN complex, we find that the *n*-Pr side chain severely clashes with a number of the water molecules forming the heptagonal water structure (Supporting Information: Figure S3b). To avoid steric clashes, these water molecules, and probably others, might be displaced from the hydration layer of the complex. It should be noted that the Et side chain of **3b** causes less water displacement than that caused by the *n*-Pr side chain of **4b**. Consequently, going from Et to *n*-Pr or *n*-Bu is anticipated to cause a positive $\Delta H_{b\text{-}solv}$ (loss of H-bonds) and a negative $-T\Delta S_{b\text{-}solv}$ (water molecules become more mobile). This could explain the enthalpic penalty and the entropic improvement of the Et→*n*-Pr/*n*-Bu transition ($\Delta H_{b\text{-}solv} > 0$, contributes unfavorably to $\Delta\Delta H_{(Et\rightarrow n\text{-}Pr/n\text{-}Bu)}$; and $-T\Delta S_{b\text{-}solv} < 0$, contributes favorably to $-T\Delta\Delta S_{(Et\rightarrow n\text{-}Pr/n\text{-}Bu)}$). Additionally, this potential influence on the hydration pattern of the S2′ pocket could explain the $COO^-$ effect on these differential thermodynamic parameters. For example, if the water displacement and disordering are more drastic in **3b**→**4b**/**5b** (absence of the $COO^-$) than in **3a**→**4a**/**5a** (presence of the $COO^-$), a more positive $\Delta H_{b\text{-}solv}$ and a more negative $-T\Delta S_{b\text{-}solv}$ are produced. These variations in $\Delta H_{b\text{-}solv}$ and $-T\Delta S_{b\text{-}solv}$ would be reflected as a more positive $\Delta\Delta H_{(Et\rightarrow n\text{-}Pr/n\text{-}Bu)}$ and a more negative $-T\Delta\Delta S_{(Et\rightarrow n\text{-}Pr/n\text{-}Bu)}$, and this is what we experimentally observe when the $COO^-$ group is absent.

The influence of the $COO^-$ group on $\Delta\Delta H_{(Et\rightarrow n\text{-}Pr/n\text{-}Bu)}$ and $-T\Delta\Delta S_{(Et\rightarrow n\text{-}Pr/n\text{-}Bu)}$ could be also explained when considering the residual organization of the water molecules hydrating the Et side chain in the unbound **3a**. As previously mentioned, this solvent organization is reduced when the Et side chain is


dx.doi.org/10.1021/jm401609a | J. Med. Chem. 2014, 57, 2315−2333

**Table 3. Differential (relative) Thermodynamic Data Caused by the Branching of the R Side Chain in the Presence and Absence of the Neighboring $COO^-$ Group**

| hydrophobic modification | presence of $COO^-$ (kJ/mol) | | | absence of $COO^-$ (kJ/mol) | | |
|---|---|---|---|---|---|---|
| Et→*i*-Pr | $\Delta\Delta H_{3a\rightarrow6a}$ = +4.6 | $-T\Delta\Delta S_{3a\rightarrow6a}$ = −5.0 | $\Delta\Delta G_{3a\rightarrow6a}$ = −0.4 | $\Delta\Delta H_{3b\rightarrow6b}$ = +6.9 | $-T\Delta\Delta S_{3b\rightarrow6b}$ = −6.1 | $\Delta\Delta G_{3b\rightarrow6b}$ = +0.8 |
| Et→*tert*-Bu | $\Delta\Delta H_{3a\rightarrow7a}$ = +13.8 | $-T\Delta\Delta S_{3a\rightarrow7a}$ = −11.7 | $\Delta\Delta G_{3a\rightarrow7a}$ = +2.1 | $\Delta\Delta H_{3b\rightarrow7b}$ = +17.6 | $-T\Delta\Delta S_{3b\rightarrow7b}$ = −15.5 | $\Delta\Delta G_{3b\rightarrow7b}$ = +2.1 |
| *n*-Pr→*i*-Bu | $\Delta\Delta H_{4a\rightarrow9a}$ = +3.9 | $-T\Delta\Delta S_{4a\rightarrow9a}$ = −3.1 | $\Delta\Delta G_{4a\rightarrow9a=+0.8}$ | $\Delta\Delta H_{4b\rightarrow9b}$ = +1.3 | $-T\Delta\Delta S_{4b\rightarrow9b}$ = −1.0 | $\Delta\Delta G_{4b\rightarrow9b}$ = +0.3 |
| *n*-Pr→neopentyl | $\Delta\Delta H_{4a\rightarrow10a}$ = +9.3 | $-T\Delta\Delta S_{4a\rightarrow10a}$ = −6.8 | $\Delta\Delta G_{4a\rightarrow10a}$ = +2.5 | $\Delta\Delta H_{4b\rightarrow10b}$ = +3.3 | $-T\Delta\Delta S_{4b\rightarrow10b}$ = −3.0 | $\Delta\Delta G_{4b\rightarrow10b}$ = +0.3 |
| *n*-Pr→*sec*-Bu | $\Delta\Delta H_{4a\rightarrow8a}$ = +6.4 | $-T\Delta\Delta S_{4a\rightarrow8a}$ = −5.4 | $\Delta\Delta G_{4a\rightarrow8a}$ = +1.0 | $\Delta\Delta H_{4b\rightarrow8b}$ = −2.6 | $-T\Delta\Delta S_{4b\rightarrow8b}$ = +2.1 | $\Delta\Delta G_{4b\rightarrow8b}$ = −0.5 |

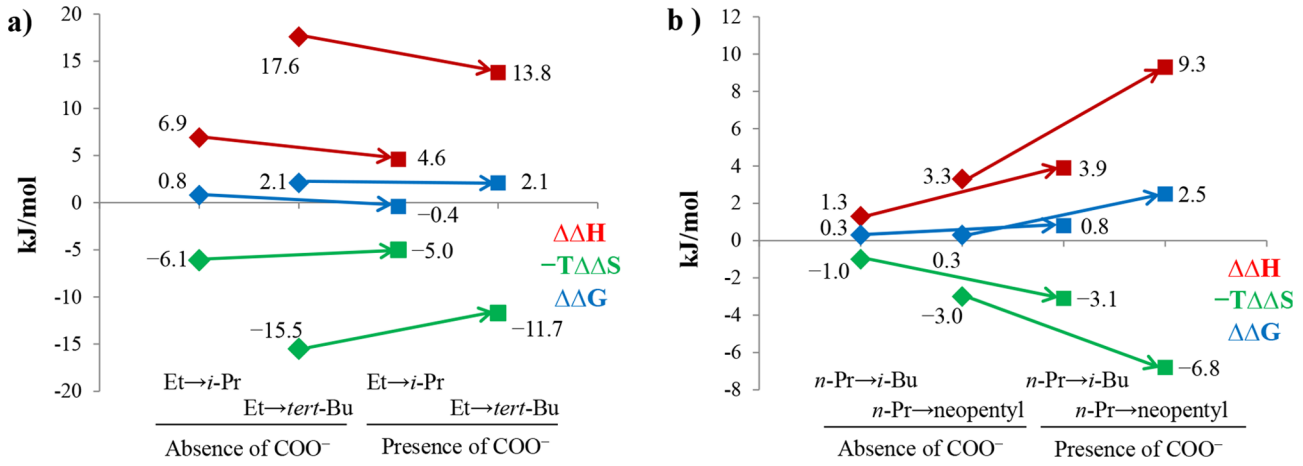


**Figure 6.** (a) The differential thermodynamic parameters of the branching of Et to *i*-Pr and *tert*-Bu, in the absence and presence of the neighboring $COO^-$ group. (b) The differential thermodynamic parameters of the branching of *n*-Pr to *i*-Bu and neopentyl, in the absence and presence of the $COO^-$. $\Delta\Delta H$ is red, $-T\Delta\Delta S$ is green, and $\Delta\Delta G$ is blue. A negative differential thermodynamic parameter indicates that the hydrophobic modification in question is favorable with regard to this parameter and vice versa. An arrow indicates how the $COO^-$ influences a differential thermodynamic parameter. An arrow going up illustrates a shift toward a more positive (unfavorable) value, and vice versa. It should be noted that while the $COO^-$ opposes the unfavorable differential enthalpy and the favorable differential entropy in the case of the Et branching, it magnifies them in the case of the *n*-Pr branching.

replaced with either *n*-Pr or *n*-Bu in the presence of the $COO^-$ ($\Delta H_{a\text{-}solv} > 0$ and $-T\Delta S_{a\text{-}solv} < 0$). However, this residual water organization is likely absent in ligand **3b** due to the absence of the $COO^-$. As a consequence, replacing the Et side chain with either *n*-Pr or *n*-Bu in the absence of the $COO^-$ occurs in the context of the already-disordered water and therefore imparts little or even no more solvent disorganization on the system ($\Delta H_{a\text{-}solv}$ is not as positive, and $-T\Delta S_{a\text{-}solv}$ is not as negative as in the presence of the $COO^-$). These less positive $\Delta H_{a\text{-}solv}$ and less negative $-T\Delta S_{a\text{-}solv}$ cause $\Delta\Delta H_{(Et\rightarrow n\text{-}Pr/n\text{-}Bu)}$ to be more positive and $-T\Delta\Delta S_{(Et\rightarrow n\text{-}Pr/n\text{-}Bu)}$ to be more negative, respectively (eqs 1B and 1C). It should be noted that the lack of any significant difference between $\Delta\Delta H_{(Et\rightarrow n\text{-}Pr)}$ and $\Delta\Delta H_{(Et\rightarrow n\text{-}Bu)}$ or between $-T\Delta\Delta S_{(Et\rightarrow n\text{-}Pr)}$ and $-T\Delta\Delta S_{(Et\rightarrow n\text{-}Bu)}$ in the absence of the $COO^-$, along with the existence of such difference in the presence of this group, further supports the hypothesis that solvent disorganization occurs in the presence but not in the absence of the $COO^-$ group.

*2. Side-Chain Branching. 2.1. Et→i-Pr/tert-Bu (an unfavorable ΔΔH and a favorable −TΔΔS opposed by the COO⁻).* Table 3 includes the differential thermodynamic data produced by the stepwise branching of the Et side chains of **3a** and **3b** to *i*-Pr and *tert*-Bu. These hydrophobic modifications are, in general, characterized by enthalpic penalties and entropic advantages which compensate each other. For example, going from an Et to *i*-Pr in the presence of the $COO^-$ gives rise to an enthalpic penalty of 4.6 kJ/mol ($\Delta\Delta H_{3a\rightarrow6a}$ = 4.6 kJ/mol) that is compensated by an entropic advantage of 5.0 kJ/mol ($-T\Delta\Delta S_{3a\rightarrow6a}$ = −5.0 kJ/mol). This compensation brings the incremental free energy change to an insignificant value ($\Delta\Delta G_{3a\rightarrow6a}$ = −0.4 kJ/mol). A further increase in the branching of the Et side chain, such as going from Et to *tert*-Bu, causes a larger enthalpic penalty (e.g., $\Delta\Delta H_{3a\rightarrow7a}$ = 13.8 kJ/mol) that is partially compensated by a larger entropic advantage (e.g., $-T\Delta\Delta S_{3a\rightarrow7a}$ = −11.7 kJ/mol). It should be noted that in the latter case, there is a net loss in binding affinity, which amounts to 2.1 kJ/mol ($\Delta\Delta G_{3a\rightarrow7a}$ = 2.1 kJ/mol), caused by the less-than-complete enthalpy−entropy compensation.

It is revealed by Table 3 and Figure 6a that the incremental thermodynamic changes caused by branching the Et group in the absence of the $COO^-$, despite having the same qualitative trend observed when the Et is branched in the presence of the $COO^-$, are more prominent. For example, the enthalpic penalties of replacing the Et with *i*-Pr and *tert*-Bu in the absence of the $COO^-$ are 6.9 and 17.6 kJ/mol, respectively (2.3 and 3.8 kJ/mol larger than the enthalpic penalties of the corresponding side chain replacements in the presence of the $COO^-$). Also, the entropic improvements in the absence of the $COO^-$ group are 6.1 and 15.5 kJ/mol (1.1 and 3.8 kJ/mol larger than the entropic improvements of the corresponding side-chain replacements in the presence of the $COO^-$). It should be noted that the impact of the $COO^-$ absence in rendering the differential enthalpy $\Delta\Delta H_{(Et\rightarrow i\text{-}Pr/tert\text{-}Bu)}$ more unfavorable and the differential entropy $-T\Delta\Delta S_{(Et\rightarrow i\text{-}Pr/tert\text{-}Bu)}$ more favorable correlates with the degree of side-chain branching (i.e., larger when the side chain is more branched: the influence on the $-T\Delta\Delta S_{(Et\rightarrow tert\text{-}Bu)}$ is 3.8 kJ/mol, while the influence on


dx.doi.org/10.1021/jm401609a | J. Med. Chem. 2014, 57, 2315−2333

$-T\Delta\Delta S_{(Et\rightarrow i\text{-}Pr)}$ is 1.1 kJ/mol). Now, how could these data be explained at the molecular level?

In presence of the $COO^-$, X-ray crystallographic data of the **3a**−TLN and **6a**−TLN complexes reveal that, upon the branching of Et to *i*-Pr, both the disappearance and the appearance of crystallographic water molecules occur. The number of the disappearing, or displaced, water molecules is, however, larger than that of the appearing, or picked up, waters. In addition, the picked-up water molecules are less interconnected by H-bond network than the displaced waters (Additional details are given in the supplementary discussions of the Supporting Information). This situation is quite similar to what happens when the Et side chain is grown to *n*-Pr (**3a**→**4a**). Given that this is the case (i.e., a net loss of water molecules and H-bonding in the **6a**−TLN complex), $\Delta H_{b\text{-}solv}$ and $-T\Delta S_{b\text{-}solv}$ are anticipated to be positive and negative, respectively. Using eqs 1B and 1C, it can be shown that $\Delta H_{b\text{-}solv}$ and $-T\Delta S_{b\text{-}solv}$ could be responsible for the experimentally observed thermodynamic data, because the positive $\Delta H_{b\text{-}solv}$ contributes unfavorably to $\Delta\Delta H_{(Et\rightarrow i\text{-}Pr)}$, and the negative $-T\Delta S_{b\text{-}solv}$ contributes favorably to $-T\Delta\Delta S_{(Et\rightarrow i\text{-}Pr)}$. Considering that the *tert*-Bu group probably displaces more water molecules than the *i*-Pr group does, $\Delta H_{b\text{-}solv}$ and $-T\Delta S_{b\text{-}solv}$ are likely larger in magnitude when the Et is replaced with *tert*-Bu (i.e., **3a**→**7a**). This was supported by modeling studies which demonstrated that the *tert*-Bu group might displace an extra water molecule, in addition to those displaced by the *i*-Pr side chain (Figure S4a, b: Supporting Information). From eqs 1B and 1C, these larger positive $\Delta H_{b\text{-}solv}$ and negative $-T\Delta S_{b\text{-}solv}$ terms cause $\Delta\Delta H_{(Et\rightarrow tert\text{-}Bu)}$ to be more unfavorable than $\Delta\Delta H_{(Et\rightarrow i\text{-}Pr)}$, and $-T\Delta\Delta S_{(Et\rightarrow tert\text{-}Bu)}$ to be more favorable than $-T\Delta\Delta S_{(Et\rightarrow i\text{-}Pr)}$. Because this matches what is observed experimentally, it could be concluded that changes in the S2′ pocket hydration pattern are likely responsible for the thermodynamic trend observed when the Et is branched to *i*-Pr and then to *tert*-Bu in the presence of the $COO^-$ (**3a**→**6a**→**7a**).

In absence of the $COO^-$, modeling studies suggest that both the *i*-Pr and the *tert*-Bu side chains of **6b** and **7b**, compared to the Et of ligand **3b**, are much more sterically incompatible with the crystallographic water molecules of the heptagonal water structure that is observed in **2a**−TLN and is assumed to be largely maintained in **3a**−TLN (Supporting Information: Figure S5a, b). It can therefore be concluded that, in the absence of the $COO^-$, the transition from the Et to either the *i*-Pr or the *tert*-Bu side chains is characterized by a positive $\Delta H_{b\text{-}solv}$ and a negative $-T\Delta S_{b\text{-}solv}$ terms, which could be responsible for the unfavorable differential enthalpy and the favorable differential entropy, respectively. It should be noted that the *tert*-Bu side chain is more sterically incompatible with the heptagonal water structure than the *i*-Pr, and this could explain why the enthalpic penalty and the entropic improvement caused by the Et→*tert*-Bu replacement are larger in magnitude than those caused by the Et→*i*-Pr replacement. This trend is qualitatively similar to what is observed when the same side-chain replacements are carried out in the presence of the $COO^-$. However, as previously mentioned, the trend is quantitatively more prominent in the absence of the $COO^-$ (i.e., absence of the $COO^-$ causes $\Delta\Delta H_{(Et\rightarrow i\text{-}Pr/tert\text{-}Bu)}$ to be more unfavorable and $-T\Delta\Delta S_{(Et\rightarrow i\text{-}Pr/tert\text{-}Bu)}$ to be more favorable). These variations could be explained in two ways:

(1) The displacement/disordering of crystallographic waters, which occurs when the Et side chain is branched to *i*-Pr or *tert*-Bu, is more costly in terms of enthalpy and more advantageous in terms of entropy when the $COO^-$ group is absent (i.e., $\Delta H_{b\text{-}solv}$ is more positive and $-T\Delta S_{b\text{-}solv}$ is more negative). Applying eqs 1B and 1C, we can conclude that a more positive $\Delta H_{b\text{-}solv}$ and a more negative $-T\Delta S_{b\text{-}solv}$ cause a more unfavorable $\Delta\Delta H_{(Et\rightarrow i\text{-}Pr/tert\text{-}Bu)}$ and a more favorable $-T\Delta\Delta S_{(Et\rightarrow i\text{-}Pr/tert\text{-}Bu)}$, and this is what is observed in the ITC data when the $COO^-$ group is absent.

(2) As previously discussed, the unbound **3a** retains some residual organization of the water molecules hydrating the Et side chain, while **3b** does not. It would therefore be anticipated that when the Et side chain in **3a** is branched to either *i*-Pr or *tert*-Bu, the residual organization of the hydration waters is gradually lost. This gives rise to a positive $\Delta H_{a\text{-}solv}$ that contributes favorably to $\Delta\Delta H_{(Et\rightarrow i\text{-}Pr/tert\text{-}Bu)}$ and a negative $-T\Delta S_{a\text{-}solv}$ that contributes unfavorably to $-T\Delta\Delta S_{(Et\rightarrow i\text{-}Pr/tert\text{-}Bu)}$. Because this residual organization of water molecules does not exist in **3b**, $\Delta H_{a\text{-}solv}$ and $-T\Delta S_{a\text{-}solv}$ are anticipated to be minimal when the Et is replaced by *i*-Pr/*tert*-Bu in the absence of the $COO^-$ group. In this case, $\Delta\Delta H_{(Et\rightarrow i\text{-}Pr/tert\text{-}Bu)}$ misses a favorable component and is shifted toward the positive, and $-T\Delta\Delta S_{(Et\rightarrow i\text{-}Pr/tert\text{-}Bu)}$ misses an unfavorable component and is shifted toward the negative.

It should be noted that the enthalpic and entropic components that might cause the $COO^-$ neighboring group effect on the thermodynamic signature of the branching of the Et side chain are the same components that might cause the $COO^-$ to have an impact on the thermodynamic signature of the homologation of the Et to either *n*-Pr or *n*-Bu side chains.

*2.2. n-Pr→i-Bu/Neopentyl (an unfavorable ΔΔH and a favorable −TΔΔS magnified by the COO⁻ group) and n-Pr→sec-Bu (an enthalpically driven effect switched to an entropically driven one by the COO⁻).* Table 3 and Figure 6b reveal that the general trend observed in the thermodynamic data of the *n*-Pr branching into *i*-Bu (**9a**/**9b**) and neopentyl (**10a**/**10b**) is qualitatively similar to the trend observed when the Et side chain is branched (enthalpic penalty and entropic improvement). However, there are two distinctive features for the *n*-Pr branching. First, the enthalpic penalty and the entropic advantage are not as large as those observed with the Et branching (e.g., $\Delta\Delta H_{4b\rightarrow 10b}$ = 3.3 kJ/mol, while $\Delta\Delta H_{3b\rightarrow 7b}$ = 17.6 kJ/mol; and $-T\Delta\Delta S_{4b\rightarrow 10b}$ = −3.0 kJ/mol, while $-T\Delta\Delta S_{3b\rightarrow 7b}$ = −15.5 kJ/mol). Second, the $COO^-$ group, which mitigates the enthalpic penalty and reduces the entropic advantage in the Et→*i*-Pr/*tert*-Bu replacement, has an opposite effect on the *n*-Pr→*i*-Bu/neopentyl replacement. For instance, when the *n*-Pr→*i*-Bu and *n*-Pr→neopentyl replacements are carried out in the presence of the $COO^-$ group, the enthalpic penalties produced are 2.6 and 6.0 kJ/mol larger than the enthalpic penalties produced by these replacements when carried out in the absence of the $COO^-$ (i.e., $\Delta\Delta H_{3a\rightarrow 9a}$ = 3.9 kJ/mol vs $\Delta\Delta H_{3b\rightarrow 9b}$ = 1.3 kJ/mol, and $\Delta\Delta H_{3a\rightarrow 10a}$ = 9.3 kJ/mol vs $\Delta\Delta H_{3b\rightarrow 10b}$ = 3.3 kJ/mol). Similarly, the entropic improvements produced by these replacements are 2.1 and 3.8 kJ/mol larger in the presence of the $COO^-$ (i.e., $-T\Delta\Delta S_{3a\rightarrow 9a}$ = −3.1 kJ/mol vs $-T\Delta\Delta S_{3b\rightarrow 9b}$ = −1.0 kJ/mol, and $-T\Delta\Delta S_{3a\rightarrow 10a}$ = −6.8 kJ/mol vs $-T\Delta\Delta S_{3b\rightarrow 10b}$ = −3.0 kJ/mol). It should be noted that the only case in which there is a significant change in the binding free energy is when the *n*-Pr is replaced with a neopentyl in the presence of the $COO^-$. In this case, the binding free energy gets worse by 2.5 kJ/mol ($\Delta\Delta G_{3a\rightarrow 10a}$ = 2.5 kJ/mol).


dx.doi.org/10.1021/jm401609a | J. Med. Chem. 2014, 57, 2315−2333

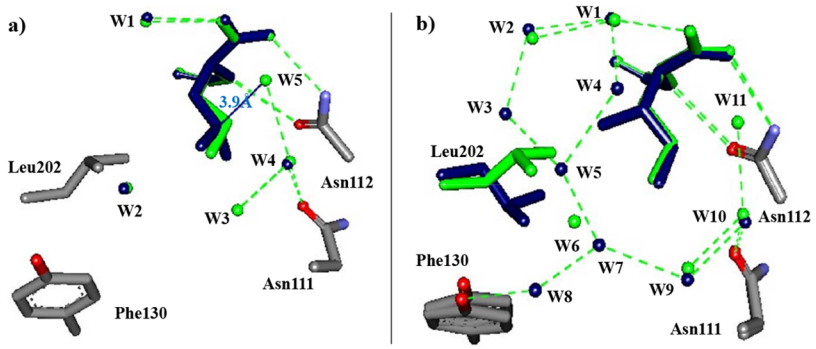


**Figure 7.** (a) Superimposition of the crystal structures of the **9a**−TLN and the **4a**−TLN complexes. Ligand **9a** and its water molecules are shown in blue. Ligand **4a** and its water molecules are shown in green. The crystal structure of the **9a**−TLN complex shows the disappearance of W3 and W5. The disappearance of these water molecules occurs because of water disordering, rather than water displacement by the side chain (e.g., the shortest distance between the *i*-Bu side chain of **9a** is outside the range of steric clashes: 3.9 Å). (b) Superimposition of the crystal structures of the **8a**−TLN and the **4a**−TLN complexes. Ligand **8a** and its water molecules are shown in blue. Ligand **4a** and its water molecules are shown in green. Significant changes in the hydration layer are observed, including the disappearance of W6 and W11, and the appearance of W3, W4, W5, W7, and W8. Also conformational change of the Leu202 side chain is observed. In both a and b, protein atoms are shown in the following colors: C (gray), O (red), and N (blue), except the Leu202 residue in b that is shown in the same color of the ligand to which it belongs.

The enthalpic penalty and the entropic advantage caused by the branching of the *n*-Pr side chain are consistent with reducing the organization of the crystallographic water molecules hydrating the P2′ side chain in the ligand−protein complex ($\Delta H_{\text{b-solv}} > 0$, contributes unfavorably to the differential enthalpy; and $-T\Delta S_{\text{b-solv}} < 0$, contributes favorably to the differential entropy). This is evidenced from the crystal structures of both **4a** and **9a**, which show that going from *n*-Pr to *i*-Bu is associated with the disappearance of a crystallographic water molecule capping the $COO^-$ group (W5: Figure 7a). The disappearance of this water molecule was previously suggested to be caused by the steric repulsion of the bulkier *i*-Bu with this water site.[15] However, a more careful analysis, which involves superimposing the two crystal structures, reveals that this proposed steric repulsion is not prominent (e.g., the shortest distance between the side chain and this water molecule is 3.9 Å, Figure 7a). It can subsequently be concluded that this water molecule likely disappears because it becomes disordered, rather than because it is displaced due to steric repulsion. The increase in the mobility of this water molecule is probably caused by reducing the strength of the H-bonds that hold it in position as a consequence of having difficulty maintaining a stable water network around the bulkier side chain of **9a**.

It is noted that the reduced incremental enthalpy/entropy of the *n*-Pr branching, relative to the Et branching, could be explained when considering that the water molecules hydrating the solvent-exposed portions of the Et side chains in the ligand−protein complexes are more organized than those hydrating these portions of the *n*-Pr side chains. These more organized waters could lose much of their organization upon the branching of the Et side chain, whereas there is not as much water organization to be lost upon the branching of the *n*-Pr. The branching of the Et, therefore, would be anticipated to elicit larger enthalpic penalties and entropic advantages than the branching of the *n*-Pr side chain. Furthermore, the shift in the thermodynamic trend of the *n*-Pr branching toward being more entropically favorable when the $COO^-$ group exists in the molecule can be explained using the same argument. For example, it was previously pointed out in the discussion of the Et→*n*-Pr replacement that the water displacement/disorganization, which occurs in the ligand−protein complex upon carrying out this hydrophobic replacement, could be less drastic in the presence of the $COO^-$. In other words, the water molecules hydrating the *n*-Pr side chain in the **4a**−TLN complex could still maintain a higher level of organization, compared to those in the **4b**−TLN complex (The $COO^-$ group could help this via electrostatic interactions and H-bonding). As a consequence, upon the branching of the *n*-Pr side chain, it would be anticipated that the hydration waters in the **4a**−TLN complex lose much of their organization, whereas the hydration waters in the **4b**−TLN complex do not have as much water organization to lose. The branching of the *n*-Pr to *i*-Bu or neopentyl, in the presence of the $COO^-$ group, would therefore produce a more positive $\Delta H_{\text{b-solv}}$ and a more negative $-T\Delta S_{\text{b-solv}}$, causing, consequently, the more unfavorable $\Delta\Delta H_{(n\text{-Pr}\rightarrow i\text{-Bu/neopentyl})}$ and the more favorable $-T\Delta\Delta S_{(n\text{-Pr}\rightarrow i\text{-Bu/neopentyl})}$ that characterize the **4a**→**9a** and the **4a**→**10a** transitions (eqs 1B and 1C).

The differential thermodynamic profile of branching the *β*-C of the *n*-Pr side chain (*n*-Pr→*sec*-Bu) is remarkable because, in the presence of the $COO^-$ group, this thermodynamic profile is entropically favorable/enthalpically unfavorable (Table 3: $\Delta\Delta H_{\text{4a}\rightarrow\text{8a}}$ = 6.4 kJ/mol, and $-T\Delta\Delta S_{\text{4a}\rightarrow\text{8a}}$ = −5.4 kJ/mol). On the other hand, in the absence of the $COO^-$, the thermodynamic profile is enthalpically favorable/entropically unfavorable (Table 3: $\Delta\Delta H_{\text{4b}\rightarrow\text{8b}}$ = −2.6 kJ/mol, and $-T\Delta\Delta S_{\text{4b}\rightarrow\text{8b}}$ = 2.1 kJ/mol). The $COO^-$ group, therefore, shifts the differential enthalpy toward the positive/unfavorable by 9.0 kJ/mol (6.4 - (−2.6) = 9.0 kJ/mol) and shifts the differential entropy toward the negative/favorable by 7.5 kJ/mol (−5.4 - 2.1 = −7.5 kJ/mol). In this study, this is the case which most prominently shows that the existence of the $COO^-$ is able to favor not only the enthalpy (e.g., H→Me) but the entropy as well, depending on the details of binding. At this moment, it might be difficult to make any inference regarding what causes the $COO^-$ to influence the thermodynamic profile in this manner. This is mainly because (1) there is no crystal structure available for any of the **4b**−TLN or the **8b**−TLN complexes till the moment; and (2) as observed in the crystal structure of the **8a**−TLN complex relative to the structure of the **4a**−TLN complex, there are quite dramatic changes in both the conformational and the hydration statuses. For example, superimposing the crystal structures of **4a**−TLN and **8a**−TLN reveals that the replacement of the *n*-Pr side chain with a *sec*-Bu


dx.doi.org/10.1021/jm401609a | J. Med. Chem. 2014, 57, 2315−2333

**Table 4. Differential (relative) Thermodynamic Data Caused by the Introduction of an Aromatic Side Chain in the Presence and Absence of the Neighboring $COO^-$ Group**

| hydrophobic modification | presence of $COO^-$ (kJ/mol) | | | absence of $COO^-$ (kJ/mol) | | |
|---|---|---|---|---|---|---|
| H→Bn | $\Delta\Delta H_{1a\rightarrow11a} = +7.1$ | $-T\Delta\Delta S_{1a\rightarrow11a} = -9.8$ | $\Delta\Delta G_{1a\rightarrow11a} = -2.7$ | $\Delta\Delta H_{1b\rightarrow11b} = +10.6$ | $-T\Delta\Delta S_{1b\rightarrow11b} = -12.9$ | $\Delta\Delta G_{1b\rightarrow11b} = -2.3$ |
| Me→Bn | $\Delta\Delta H_{2b\rightarrow11a} = +12.7$ | $-T\Delta\Delta S_{2a\rightarrow11a} = -10.3$ | $\Delta\Delta G_{2a\rightarrow11a} = +2.4$ | $\Delta\Delta H_{2b\rightarrow11b} = +9.1$ | $-T\Delta\Delta S_{2b\rightarrow11b} = -9.6$ | $\Delta\Delta G_{2b\rightarrow11b} = -0.5$ |
| Me→2-thienylmethyl | $\Delta\Delta H_{2a\rightarrow12a} = +12.7$ | $-T\Delta\Delta S_{2a\rightarrow12a} = -11.1$ | $\Delta\Delta G_{2a\rightarrow12a} = +1.6$ | $\Delta\Delta H_{2b\rightarrow12b} = +8.8$ | $-T\Delta\Delta S_{2b\rightarrow12b} = -9.5$ | $\Delta\Delta G_{2b\rightarrow12b} = -0.7$ |

causes the disappearance of two water molecules (W6 and W11: Figure 7b) and the appearance of five others (W3, W4, W5, W7, and W8: Figure 7b). What significantly helps the appearance/acquisition of the five water molecules by the complex is the conformational change occurring in the side chain of Leu202 residue. This conformational change occurs to avoid steric clash with the additional $CH_3$ introduced in the ligand side chain when the *n*-Pr is replaced by *sec*-Bu. Such change opens up space for the incoming water molecules and thereby facilitates the formation of the interconnected water network shown in Figure 7b.

Translating these crystallographic finding into thermodynamic changes, we can find that the disappearance of some water molecules causes a positive $\Delta H_{\text{b-Wdisp}}$ and a negative $-T\Delta S_{\text{b-Wdisp}}$ terms, while the acquisition of other water molecules causes a negative $\Delta H_{\text{b-Wstrct}}$ and a positive $-T\Delta S_{\text{b-Wstrct}}$ terms. Given that going from **4a** to **8a** produces an unfavorable differential enthalpy and favorable differential entropy, it might be concluded that the thermodynamic terms produced by the water disappearance outweigh the terms produced by the water acquisition. However, this might not be the case if the conformational change of Leu202 yields significant thermodynamic terms that might shift the differential parameters one way or another. For example, rather than assuming that $\Delta H_{\text{b-Wdisp}}$ outweighs $\Delta H_{\text{b-Wstrct}}$ and produces the unfavorable $\Delta\Delta H_{(n\text{-Pr}\rightarrow sec\text{-Bu})}$, $\Delta H_{\text{b-Wstrct}}$ might be the predominant hydration term and a positive $\Delta H_{\text{b-Conf}}$ (the enthalpic contribution of the conformational change) might outweigh it causing the unfavorable $\Delta\Delta H_{(n\text{-Pr}\rightarrow sec\text{-Bu})}$. It is worth mentioning that modeling experiments suggest that the Leu202 conformational change, which occurs in the **8a**−TLN complex, might not take place in the **8b**−TLN. If this is verified by X-ray crystallography, the additional conformational thermodynamic terms of the **4a**→**8a** transition will most likely be responsible for a significant deal of the influence of the $COO^-$ group on the thermodynamic profile of the *n*-Pr→*sec*-Bu replacement. The binding of ligands **8a** and **8b** will be further discussed in subsequent studies in the light of the ongoing investigations.

*3. Introduction of an Aromatic Group. 3.1. Me→Bn/2-Thienylmethyl (an unfavorable ΔΔH magnified by the $COO^-$).* Table 4 includes the differential thermodynamic data produced by introducing an aromatic moiety in the R side chain. It is noted that growing the Me side chain to Bn produces thermodynamic profiles that are almost identical to those produced by growing the Me to 2-thienylmethyl. Consequently, it might be sufficient for this section to discuss the hydrophobic modifications involving the Bn side chain.

In the presence of the $COO^-$, going from Me→Bn (**2a**→**11a**) causes an enthalpic penalty and an entropic improvement which do not completely compensate each other ($\Delta\Delta H_{2a\rightarrow11a}$ = 12.7 kJ/mol, $-T\Delta\Delta S_{2a\rightarrow11a} = -10.3$ kJ/mol). This incomplete enthalpy−entropy compensation causes a net unfavorable binding free energy change ($\Delta\Delta G_{2a\rightarrow11a}$ = 2.4 kJ/mol). In the absence of the $COO^-$, a smaller enthalpic penalty is observed ($\Delta\Delta H_{2b\rightarrow11b}$ = 9.1 kJ/mol). This smaller enthalpic penalty is completely compensated by an entropic improvement, bringing the free energy change to an insignificant value ($-T\Delta\Delta S_{2b\rightarrow11b} = -9.6$ kJ/mol, $\Delta\Delta G_{2b\rightarrow11b} = -0.5$ kJ/mol). Taken together, these thermodynamic data indicate that the $COO^-$ group causes both the differential enthalpy and the differential free energy to become more unfavorable by 3.6 and 2.9 kJ/mol, respectively, as the side chain is enlarged. Previously, it has been shown that carrying out the H→Me replacement in the presence of the $COO^-$ causes both the differential enthalpy and the differential free energy to become more favorable by 7.2 and 3.4 kJ/mol, respectively. It is therefore apparent that the beneficial effect of the $COO^-$ group on both the incremental enthalpy and free energy changes of the H→Me replacement is partially counteracted by a detrimental effect on these thermodynamic parameters when the Me is grown to a Bn side chain. This pattern of change in the $COO^-$ influence on the thermodynamic signature of the hydrophobic side-chain replacement is apparently similar to the change in the $COO^-$ group effect observed when the H is replaced with Me then Et (advantageous then detrimental effects on both the differential enthalpy and the differential free energy). The two apparently similar patterns are, however, achieved in different ways. For example, Figure 8 reveals that, in the H→Me→Bn, a larger improvement in enthalpy, followed by a larger penalty, occurs in the presence of the $COO^-$. On

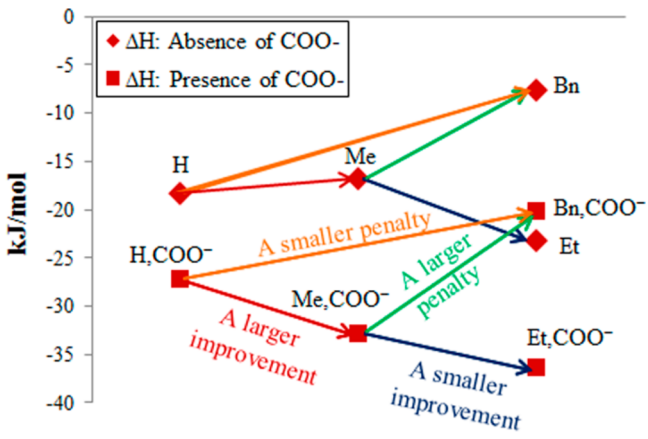


**Figure 8.** The enthalpic data obtained from ITC experiments for ligands **1a**, **2a**, **3a**, and **11a** (H/Me/Et/Bn, $COO^-$), in comparison with the data of ligands **1b**, **2b**, **3b**, and **11b** (H/Me/Et/Bn). Arrows indicate the changes that Δ*H*s undergo when the hydrophobic modifications in question are carried out: An arrow going up represents an enthalpic penalty (ΔΔ*H* is positive), while one going down represents an improvement (ΔΔ*H* is negative). Statements comparing the differential enthalpies in the presence vs absence of the $COO^-$ are made next to the arrows associated with the presence of the $COO^-$. A "larger" and a "smaller" descriptions are mentioned relative to the absence of the $COO^-$ case. Attention needs to be paid to how steep the arrows are in order to perceive the comparisons.


dx.doi.org/10.1021/jm401609a | *J. Med. Chem.* 2014, 57, 2315−2333

the other hand, in the H→Me→Et, a larger, followed by a smaller, improvement in enthalpy occurs in the presence of this group (larger and smaller are mentioned in the context of a comparison with the absence of the $COO^-$ case).

This different way in achieving the same effect, combined with the fact that going from the Me to the Et side chain does not seem to significantly impact the hydration pattern of the S2′ pocket while going from Me→Bn does, indicates that the molecular basis for the $COO^-$ effect in both cases is different. Close investigation of the crystal structure of **11a**−TLN, relative to **2a**−TLN, reveals that most of the crystallographic waters in the S2′ pocket region are displaced when the Me is replaced with Bn (i.e., W2, W4, W5, and W6: Figure 9). The

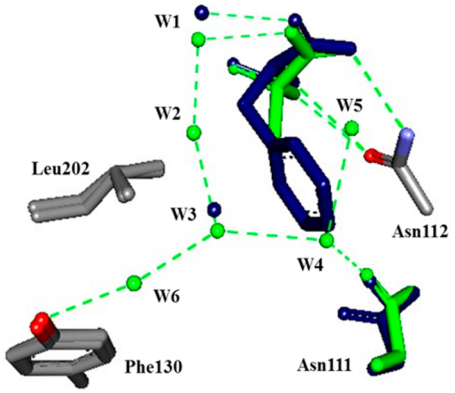


**Figure 9.** Superimposition of the crystal structures of the **11a**−TLN and the **2a**−TLN complexes. Ligand **11a** and its water molecules are shown in blue. Ligand **2a** and its water molecules are shown in green. The crystal structure of the **11a**−TLN complex shows the disappearance of W2, W4, W5, and W6. The disappearance of most of these water molecules occurs because of water displacement by the side chain. Protein atoms are shown in the following colors: C (gray), O (red), and N (blue), except the Asp111 residue that is shown in the same color of the ligand to which it belongs (its C═O has two conformations).

exception to this is W3 which is probably stabilized by π···H−O hydrogen bonding with the phenyl ring.[30−32] It is anticipated that similar hydration changes occur in the ligand−protein complex when the Me side chain is replaced by Bn in the absence of the $COO^-$. For example, the Bn side chain would not be sterically compatible with most of the crystallographic water molecules; consequently, these water molecules are anticipated to be displaced in the **11b**−TLN. In addition, a water molecule, similar to W3, could be stabilized by the phenyl ring: The $COO^-$ group of the **11a**−TLN does not seem to participate in stabilizing this water molecule; consequently, the absence of this group from the **11b**−TLN would not be anticipated to reduce the chance of stabilizing this water molecule.

It should be noted that, even though the final states of both the **2a**−TLN→**11a**−TLN and the **2b**−TLN→**11b**−TLN transitions (i.e., the **11a**−TLN and the **11b**−TLN) are quite similar with regard to their hydration statuses, the initial states (i.e., the **2a**−TLN and the **2b**−TLN) are not. For example, it is likely that the water network in the S2′ region of the **2a**−TLN complex preserves more favorable intrinsic enthalpy than the water network of the **2b**−TLN does [Note: intrinsic enthalpy is used here in a sense that considers the gas phase as the reference]. This is because of the presence of the $COO^-$ group in the **2a**−TLN complex, which is capable of strengthening its adjacent H-bond network. Having mentioned this, the transition **2a**−TLN→**11a**−TLN would involve losing this additional favorable intrinsic enthalpy, and consequently its $\Delta H_{b\text{-}solv}$ term would be more positive than the $\Delta H_{b\text{-}solv}$ term of the **2b**−TLN→**11b**−TLN transition. Applying eq 1B, it can be concluded that the differential enthalpy of **2a**−TLN→**11a**−TLN would be more unfavorable than the differential enthalpy of **2b**−TLN→**11b**−TLN, and this is what we observe in the experimental data.

Going back a step and investigating the transitions **1a**−TLN→**11a**−TLN and **1b**−TLN→**11b**−TLN, we find that crystallographic waters are displaced (e.g., Figure S6: Supporting Information) giving rise to positive $\Delta H_{b\text{-}solv}$ terms and, in turn, unfavorable differential enthalpies (Table 4: $\Delta\Delta H_{1a\rightarrow 11a}$ = 7.1 kJ/mol, and $\Delta\Delta H_{1b\rightarrow 11b}$ = 10.6 kJ/mol). These positive $\Delta H_{b\text{-}solv}$ terms and the unfavorable differential enthalpies are accompanied by negative $-T\Delta S_{b\text{-}solv}$ terms and favorable differential entropies ($-T\Delta\Delta S_{1a\rightarrow 11a}$ = −9.8 kJ/mol, and $-T\Delta\Delta S_{1b\rightarrow 11b}$ = −12.9 kJ/mol). It should be noted that the $COO^-$ in this side-chain replacement (i.e., H→Bn) causes the unfavorable enthalpy to become less unfavorable (e.g., Figure 8), and the favorable entropy to become less favorable. This observation is in agreement with the previous discussion of the replacement of H with Me side chain, in which it was pointed out that the displacement of ordered water molecules from the S2′ pocket of the **1a**−TLN produces smaller enthalpic penalty and entropic advantage than the displacement of waters from the **1b**−TLN (e.g., because of the disrupted water network in the S2′ pocket of the **1a**−TLN complex: Figure S6, Supporting Information). In the H→Me replacement, however, the enthalpic penalties and the entropic advantages contributed by water displacement are neutralized or even overwhelmed by the enthalpic advantages and the entropic penalties contributed by the acquisition of water molecules from the bulk phase (e.g., unlike the H→Bn replacement, in which the acquisition of water from the bulk is anticipated to be very limited due to the bulkiness of the Bn side chain). The ITC data of the ligands with the Bn side chain, therefore, provide additional support to the model used to explain the thermodynamic data of the ligands discussed in ref 16.

**Enthalpy−Entropy Compensation.** Plotting the enthalpic vs the entropic data of the 24 ligands shows that for all of the studied ligands except **1a**, **1b**, and **2b**, a linear enthalpy−entropy compensation relation is at work (Figure 10). The slope of this linear relation deviates from unity (= −1.27) and therefore indicates that the compensation is not complete. This deviation is in favor of the enthalpy. For example, a change in $-T\Delta S$ which amounts to 1.00 kJ/mol is accompanied by a change in $\Delta H$ of 1.27 kJ/mol in the opposite direction (if $-T\Delta S$ is unfavorable, $\Delta H$ is favorable, and vice versa). As a consequence of this, $\Delta G$ would change by 0.27 kJ/mol in the same direction of the enthalpy. It is likely that the remarkable enthalpy−entropy compensation relation depicted in Figure 10 is obtained because the major factor that causes the incremental thermodynamic changes is the change in the organization/H-bonding status of the hydration waters in both the unbound and the complexed states. If all other factors are considered negligible or cancel each other, the relationship obtained from Figure 10 (i.e., $\Delta\Delta H = -1.26\ (-T\Delta\Delta S)$) can be used to write eq 2 when $\Delta\Delta H$ is substituted with $(\Delta H_{b\text{-}solv} - \Delta H_{a\text{-}solv})$, and $-T\Delta\Delta S$ is substituted with $(-T\Delta S_{b\text{-}solv} - (-T\Delta S_{a\text{-}solv}))$. It is apparent that the relation in eq 2 could be achieved if the


dx.doi.org/10.1021/jm401609a | J. Med. Chem. 2014, 57, 2315−2333

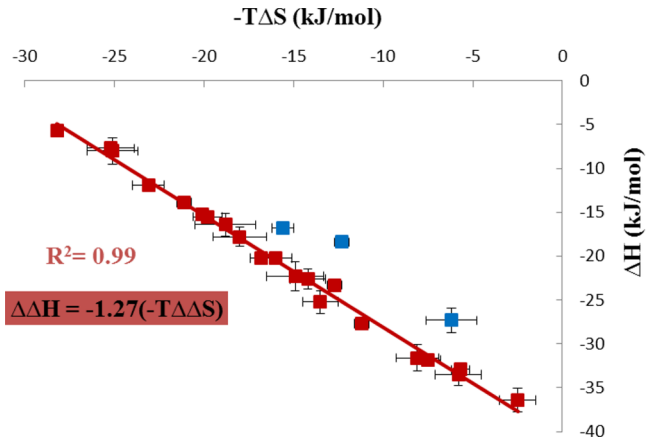


**Figure 10.** A plot of the $\Delta H$ vs $-T\Delta S$ data of the 24 ligands studied herein. The plot shows a generalized enthalpy−entropy compensation relation (improved binding entropy is accompanied by worsened binding enthalpy, and vice versa). Excluding ligands **1a**, **1b**, and **2b**, the enthalpy−entropy compensation is linear with an $R^2$ value of 0.99. The linear relationship reveals that for each 1.00 kJ/mol change in $-T\Delta S$, the binding enthalpy and the binding free energy change by 1.27 and 0.27 kJ/mol, respectively, in a direction opposite to the change of $-T\Delta S$. Going from any of the 21 ligands to **1a**, **1b**, or **2b** would cause enthalpy and free energy changes which are less favorable (or more unfavorable) than what would be expected based on the linear trend, and vice versa.

change in the organization/H-bonding status of the hydration waters, regardless of whether these waters belong to the unbound or the complexed state, produces an enthalpy−entropy compensation which follows a linear trend with a slope of "1.27" (e.g., $\Delta H_{\text{b-solv}}/\Delta H_{\text{a-solv}} = -1.27(-T\Delta S_{\text{b-solv}}/-T\Delta S_{\text{a-solv}}) + a/b$, where $a$ and $b$ are the constants of the linear equations of the complexed and the uncomplexed states, respectively). It should be noted, however, that caution should be exercised in applying this relationship to other ligand−protein systems because other factors might be at work, or the changes in the organization/H-bonding status of the hydration waters might follow a different enthalpy−entropy compensation pattern. Even within the series studied herein, ligands **1a**, **1b**, and **2b** were noticed to be outliers (Figure 10).

$$\Delta H_{\text{b-solv}} - \Delta H_{\text{a-solv}} = -1.27(-T\Delta S_{\text{b-solv}} - (-T\Delta S_{\text{a-solv}})) \quad (2)$$

The enthalpy−entropy compensation observed in this study, with its tendency to favor the binding free energy when the enthalpy is more beneficial, may be related to the concept of the enthalpically guided free energy optimization.[33−35] Although this concept has been recently challenged,[36] and there is nothing that requires structural modifications with improved enthalpies to have greater opportunities to yield improved binding free energies than structural modifications with improved entropies, the case presented in this study may be viewed as a remarkable case in which this concept may apply. In some ligand modifications, however, we may still encounter a large entropic penalty which can offset any binding affinity advantage obtained due to enthalpic improvement. For example, consider going from one of the "well-behaved" ligands to a more enthalpically favorable ligand in the **1a**, **1b**, and **2b** ligand set. This enthalpic optimization is accompanied by a larger entropic penalty than what would be produced if the former ligand went to another "well-behaved" ligand having the same enthalpic advantage. This larger entropic penalty causes the free energy change to be less advantageous, and consequently this ligand modification is not desirable even though it is enthalpically favorable. It should be noted that the opposite is true: going from a ligand in the **1a**, **1b**, and **2b** set to one of the "well-behaved" ligands is desirable because it is more efficient in terms of binding free energy improvement, even if the entropy, rather than the enthalpy, is the thermodynamic parameter which improves (the accompanying enthalpic penalty would be smaller than what is anticipated).

## CONCLUSIONS

In this study, the influence of a neighboring $COO^-$ group on the thermodynamic signature of the hydrophobic binding to the shallow, flat, and solvent-exposed S2′ pocket of TLN was investigated. Two series with twelve phosphonamidate TLN inhibitors in each, which differ only in the presence of the terminal $COO^-$ group, were designed and synthesized. Within each series, the P2′ hydrophobic side chain that is adjacent to the terminal $COO^-$ was changed in a systematic manner which explores various types of hydrophobic modifications (e.g., side-chain homologation, branching, and incorporating a bulky aromatic moiety). ITC was used to determine the thermodynamic signature of each ligand and the incremental (differential) thermodynamic profiles of ligand pairs, each of which includes a ligand that is modified to the other through carrying out one of the previously mentioned hydrophobic modifications. These differential thermodynamic profiles were compared in the presence and absence of the $COO^-$ group in order to identify the effect of this $COO^-$ on the thermodynamics of the hydrophobic binding. The $COO^-$ group was found to modulate these profiles in most cases. For example, the presence of this group caused the differential enthalpy to become more favorable/less unfavorable and the differential entropy to become more unfavorable/less favorable in the case of the replacement of H with Me, the homologation of the Et to *n*-Pr/*n*-Bu, and the branching of the Et to *i*-Pr/*tert*-Bu. On the other hand, the $COO^-$ was found to cause the differential enthalpy to become less favorable/more unfavorable and/or the differential entropy to become less unfavorable/more favorable in the case of the Me homologation to Et, the branching of the *n*-Pr to *sec*-Bu/*i*-Bu/neopentyl, and the incorporation of an aromatic moiety in the P2′ side chain (Me→Bn/2-thienylmethyl). The influence of the $COO^-$ on the differential binding free energy was, however, limited to two or three cases in which the $COO^-$ caused the differential binding energy to be either more or less favorable (the H→Me vs the Me→Et and the Me→Bn/2-thienylmethyl replacements).

Furthermore, the effect of the $COO^-$ group on the thermodynamic signatures of the hydrophobic side-chain modifications was rationalized using a model which considers the organization/H-bonding status of the water molecules hydrating the P2′ side chain in the unbound and the complexed states to be variable according to the local environment. In this model, the hydration waters are assumed to encounter difficulty in maintaining a highly organized hydration cluster at the side chain/water interface when this side chain increases in size or becomes more branched. The $COO^-$ group likely opposes this disorganization/loss of H-bonding of the hydration waters through its ability to participate in H-bonding with these waters. The presence of the $COO^-$ could therefore modulate how much water organization/H-bonding is reduced in each hydrophobic modification. This, in turn, causes the differential

thermodynamic signatures of hydrophobic modifications to vary based on whether or not the $COO^-$ group exists in the molecule. A notable example which illustrates how this model is capable of explaining the incremental thermodynamic data obtained from the ITC experiments is the Me→Et replacement. Given that water disorganization/loss of H-bonding in the unbound state causes the differential enthalpy to be more favorable, this effect, being unopposed in the absence of the $COO^-$ and opposed in its presence, causes the Me→Et replacement to become more enthalpically favorable in the absence of this group. The same principles apply when the complexed state is considered. For example, more ordered waters are displaced or become less organized when the side chain increases in size or become more branched. Also, the amount of water displaced from the complex could vary depending on whether the $COO^-$ group is present or not. The incremental thermodynamic signatures of hydrophobic modifications and the influence of the $COO^-$ group on theses signatures, therefore, represent the outcomes of the complex interplay between the changes in the hydration statuses of the unbound and the complexed ligands.

Another remarkable finding in this study is that most of the ligands show an enthalpy−entropy compensation relationship which follows a linear trend with a slope indicating that there is a net improvement in the binding free energy obtained when the enthalpy is improved (enthalpy guided optimization of binding affinity). This thermodynamic behavior was attributed to the prominent role the hydration changes play in determining the differential thermodynamic profiles of these hydrophobic modifications. Enthalpy-guided optimization of binding affinity, however, might not be a universal concept that can be applied in all cases. For example, even within the series studied herein, three ligands showed that the advantageous binding free energy obtained from improving the enthalpy could be offset by the entropic penalty.

There are a number of general conclusions that the study presented herein suggests. First, the hydrophobic effect should not be confined to a narrow area of molecular explanations, such as being driven by releasing the structured water from the ligand−water interface or releasing disordered waters from protein cavities. Rather, all aspects of the hydrophobic binding should be considered carefully and evaluated on a case-by-case basis. Second, the thermodynamic signature of the hydrophobic effect could be greatly influenced by the neighboring groups; consequently, the hydrophobic effect is very dependent on what other functionalities the ligand and/or the ligand−protein complex have. Third, a complex interplay between the hydration statuses of the unbound ligand and the ligand−protein complex could dominate the thermodynamic signature of the hydrophobic effect, particularly when the protein pocket, in which the hydrophobic side chain being modified binds, is shallow, flat, and solvent-exposed (e.g., the S2′ pocket of TLN). Fourth, enthalpy−entropy compensation is a predominant phenomenon in ligand−protein binding, which needs to be overcome in order to gain improvement in binding. When the ligand−protein system behaves well in terms of its thermodynamics, the enthalpy−entropy compensation might be overcome via optimizing one of the thermodynamic parameters (e.g., the enthalpy). Fifth, studies in which ITC and other experimental techniques are used to obtain information about ligand−protein binding could be useful in setting the stage toward better understanding of the fundamental concepts of this phenomenon. This improved understanding could lead to important advances in many areas in which molecular recognition is a major player. For example, an improved understanding of hydrophobic binding may provide new insights into the relatively undeveloped field of designing potent small molecule protein−protein interaction antagonists. When presented with a shallow, flat, and solvent-exposed hydrophobic pocket on the protein host in a target protein−protein interaction system, a careful consideration of the ability of potential neighboring ligand groups to modify the relative enthalpy and entropy status of water molecules that interact with the unbound ligand vs the bound complex could lead to potent ligand designs which would not otherwise be considered. Finally, it is important to note that the explanations provided in the current study to the thermodynamic data presented herein could serve as bases for additional experimental and/or theoretical studies geared toward revealing more about the role water and hydrophobic effects play in ligand binding.

## EXPERIMENTAL SECTION

**Chemistry.** *General Methods.* Reagents were obtained from commercial suppliers and used without further purification. Anhydrous solvents were purchased as sealed bottles from either Fisher-Acros (Carousal) or Aldrich (Sure-seal) and were maintained under an argon atmosphere. Tetrahydrofuran (THF) was distilled from a sodium/benzophenone still and used immediately. Dichloromethane (DCM) was distilled from a calcium hydride still and used immediately. Solvent removal was performed on a rotary evaporator equipped with a 20−60 °C water bath and a self-contained aspirator. Thin-layer chromatography (TLC) was performed on Analtech (Newark, DE) 200 μm Silica Gel F coated on polyethylene sheets. Visualization was accomplished with 254 nm UV light or iodine staining. The silica gel used in the flash chromatography was 40−75 μm flash grade purchased from Sorbent Technologies (Atlanta, GA). All amino acids used are L unless otherwise noted. Proton, phosphorus, and carbon nuclear magnetic resonance was performed in deuterated solvents purchased from Cambridge Isotope Laboratories, Inc. (Andover, MD) on one of the following instruments: Varian Gemini 300 MHz, Varian Inova 400 MHz, or Varian Inova 500 MHz. $^1H$ NMR data are reported in the following format: chemical shift (ppm values in relation to TMS or appropriate solvent peak), multiplicity (s = singlet, d = doublet, t = triplet, q = quartet, dd = doublet of doublet, dt = doublet of triplet, dq = doublet of quartet, m = multiplet, brs = broad singlet), coupling constant(s), and integration. Whenever fractions of chemically equivalent protons appear at widely spaced chemical shifts, such as when the compound exists in multiple conformations, the chemical shifts are reported, followed by the multiplicity(ies) preceded by the number of peaks (e.g., 2 s, 2 d, etc.), the coupling constant(s), and the sum of the integrations of these peaks. Low resolution ESI mass spectrometry was performed on a Thermo Finnigan LCQ Advantage instrument using 60% methanol in water with 1% acetic acid or 60% acetonitrile in water with 0.1% trifluoroacetic acid as the mobile phase. Preparative and semi-preparative HPLC instrumentation included a Milton Roy gm4000 gradient programmer, Milton Roy Constametric I and III pumps, a Rheodyne 7125 injector with a 5.00 mL sample loop, and a Knauer Variable Wavelength Detector set at either 218 or 254 nm with a preparative flow cell. The HPLC column used was a Phenomenex LUNA C18(2), 5 μm, 100A pore, 21 mm × 250 mm with Security Guard cartridge used with a flow rate of 8 mL/min. All final compounds were at least 95% pure by HPLC analysis. The HPLC analysis of the final compounds involved the use of acetonitrile/water as a mobile phase in a gradient elution method (10→90% acetonitrile over 14 min).

Details of the synthesis of ligands **5a**, **9a**, **5b**, and **9b** are given below. The synthesis and the characterization of the other ligands are described in the Supporting Information.

*Synthesis of Benzyl N-(Hydroxymethyl)carbamate (**1**).*[37] Benzyl carbamate (6.0 g, 40 mmol) was added to a solution of 37% formalin (4.4 g, 56 mmol) and sodium carbonate (2.2 g, 20 mmol) in 65 mL of water. The mixture was heated until all the solids were dissolved, cooled to room temperature, and stirred overnight. The precipitated solid was then filtered, dried, and redissolved in dichloromethane. The solution was dried using anhydrous magnesium sulfate, and the solvent was removed under vacuum to give the product as a white solid which was used in the next step without further purification (5.4 g, 74%): $^1$H NMR ($CDCl_3$) $\delta$ 4.10 (s, 1H), 4.71 (d, $J$ = 6.5 Hz, 2H), 5.13 (s, 2H), 6.07 (s, 1H), 7.36 (s, 5H); $m/z$ (LCMS, ESI): found 182.2 $[M + H]^+$, $[C_9H_{11}NO_3 + H]^+$ requires 182.1.

*Synthesis of Benzyl N-(Acetoxymethyl)carbamate (**2**).* Compound **1** (3.6 g, 20 mmol) was dissolved in 25 mL of anhydrous THF and was added slowly to an ice-cooled stirred solution of 23 mL of acetic anhydride and 6.5 mL of anhydrous pyridine under argon. The mixture was stirred at rt for 2 h, and then the solution was diluted with 150 mL of ethyl acetate and washed with 1 M HCl (3 × 150 mL) and brine (2 × 150 mL). The organic layer was dried with anhydrous magnesium sulfate, and the volatile materials were removed under vacuum to give an oily residue which was purified with flash chromatography (3.0 g, 67%) of the pure product. $^1$H NMR ($CDCl_3$) $\delta$ 2.08 (s, 3H), 5.16 (s, 2H), 5.23 (d, $J$ = 7.5 Hz, 2H), 6.08 (s, 1H), 7.38 (s, 5H); $m/z$ (LCMS, ESI): found 246.0 $[M + Na]^+$, $[C_{11}H_{13}NO_4 + Na]^+$ requires 246.1.

*Synthesis of Dimethyl N-(Benzyloxycarbonyl)-aminomethylphosphonate (**3**).* A mixture of compound **2** (2.9 g, 13 mmol) and trimethyl phosphite (4.6 mL, 39 mmol) was refluxed for 3 h. The volatile materials were removed by distillation at 60 °C under reduced pressure to give the product as an oily residue which was used in the next step without further purification (3.4 g, 97%) $^1$H NMR ($CDCl_3$) $\delta$ 3.62 (dd, $J$ = 6.5 Hz, $J_{H-P}$ = 11.0 Hz, 2H), 3.72 (d, $J_{H-P}$ = 11.0 Hz, 6H), 5.09 (s, 2H), 5.83 (s, 1H), 7.25−7.40 (m, 5H), $^{31}$P NMR ($CDCl_3$) $\delta$ 25.32; $m/z$ (LCMS, ESI): found 296.1 $[M + Na]^+$, $[C_{11}H_{16}NO_5P + Na]^+$ requires 296.1.

*Synthesis of Methyl N-(Benzyloxycarbonyl)-aminomethylphosphonate (**4**).* Compound **3** (3.3 g, 12 mmol) was shook vigorously with 10% NaOH (14.5 mL, 3 equiv) until it was completely dissolved. The mixture was stirred at room temperature for 2 h and then diluted with water, extracted with ethyl acetate (2 × 30 mL), and acidified to pH 1 with 2 M HCl. The aqueous solution was extracted with dichloromethane (2 × 100 mL) and ethyl acetate (2 × 50 mL). The dichloromethane layers were combined, washed with brine (2 × 50 mL), and dried using anhydrous magnesium sulfate. The ethyl acetate layers were also combined, washed with brine (2 × 25 mL), and dried with anhydrous magnesium sulfate. The two organic layers were then combined, and the volatile solvents were removed under high vacuum to give the product as a pure white solid (2.3 g, 73%). $^1$H NMR ($CDCl_3$) $\delta$ 3.64 (d, $J_{H-P}$ = 11.0 Hz, 2H), 3.71 (d, $J_{H-P}$ = 11.0 Hz, 3H), 5.12 (s, 2H), 5.7 (brs, 1H), 7.28−7.42 (m, 5H), 11.8 (brs, 1H), $^{31}$P NMR ($CDCl_3$) $\delta$ 24.12; $m/z$ (LCMS, ESI): found 282.1 $[M + Na]^+$, $[C_{10}H_{14}NO_5P + Na]^+$ requires 282.1.

*General Procedure for Amide Coupling. Intermediates **i5a**, **i9a**, **i5b**, and **i9b**.* To a cooled solution of Boc-L-leucine (1.0 equiv), the amine/$\alpha$-amino ester HCl (1.2−1.5 equiv), and PyBop 1.2 equiv (or EDCI·HCl 1.2 equiv and HOBt 1.2 equiv) in anhydrous DMF was added diisopropylethylamine (3.3−4.0 equiv) gradually. The reaction mixture was stirred at room temperature for 5 h to overnight, diluted with ethyl acetate (50 mL for every 5 mL of DMF), and then extracted with 1 M HCl (3×), saturated sodium bicarbonate (3×), and brine (2×). The organic layer was then dried with anhydrous sodium sulfate, and the solvent was evaporated under vacuum to give the products which were purified by flash chromatography whenever needed.

*(N-(tert-Butoxycarbonyl)-L-leucinyl)-L-norleucine Methyl Ester (**i5a**).* Following the general procedure for amide coupling, Boc-L-leucine (579 mg, 2.5 mmol) was reacted with norleucine methyl ester hydrochloride (545 mg, 3.0 mmol: synthesized in-house) in anhydrous DMF (10 mL), using EDCI.HCl (573 mg, 3.0 mmol) and HOBt (405 mg, 3.0 mmol) as coupling reagents and diisopropylethylamine (1.07 g, 8.25 mmol) as a base. A 680 mg amount of compound **i5a** was obtained after purification with flash chromatography (76%). $^1$H NMR (DMSO-$d_6$) $\delta$ 0.80−0.90 (m, 9H), 1.35 (s, 9H), 1.20−1.50 (m, 6H), 1.50−1.72 (m, 3H), 3.58 (s, 3H), 3.97 (q, 1H), 4.22 (q, 1H), 6.82 (d, $J$ = 8.5 Hz, 1H), 8.05 (d, $J$ = 6.5 Hz, 1H); $m/z$ (LCMS, ESI): found 381.1 $[M + Na]^+$, $[C_{18}H_{34}N_2O_5 + Na]^+$ requires 381.2.

*((S)-2-(tert-Butoxycarbonylamino)-4-methylpentanoyl)-L-leucine Methyl Ester (**i9a**).* Following the general procedure for amide coupling, Boc-L-leucine (578 mg, 2.5 mmol) was reacted with L-leucine methyl ester hydrochloride (545 mg, 3.0 mmol) in anhydrous DMF (10 mL), using PyBop as a coupling reagent (1.56 g, 3.0 mmol) and diisopropylethylamine (1.07 g, 8.25 mmol) as a base. A 726 mg amount of compound **i9a** was obtained after purification with flash chromatography (81%). $^1$H NMR (DMSO-$d_6$) $\delta$ 0.80−0.92 (m, 12H), 1.37 (s, 9H), 1.35−1.42 (m, 2H) 1.42−1.52 (m, 1H), 1.53−1.70 (m, 3H), 3.60 (s, 3H), 3.97 (q, 1H), 4.27−4.35 (m, 1H), 6.83 (d, $J$ = 8.5 Hz, 1H), 8.11 (d, $J$ = 7.5 Hz, 1H); $m/z$ (LCMS, ESI): found 381.1 $[M + Na]^+$, $[C_{18}H_{34}N_2O_5 + Na]^+$ requires 381.2.

*(S)-2-(tert-Butoxycarbonylamino)-4-methyl-N-pentylpentanamide (**i5b**).* Following the general procedure for amide coupling, Boc-L-leucine (578 mg, 2.5 mmol) was reacted with $n$-pentylamine (261 mg, 3.0 mmol) in anhydrous DMF (10 mL), using EDCI·HCl (573 mg, 3.0 mmol) and HOBt (405 mg, 3.0 mmol) as coupling reagents and diisopropylethylamine (1.07 g, 8.25 mmol) as a base. A 593 mg amount of compound **i5b** was obtained after purification with flash chromatography (79%). $^1$H NMR (DMSO-$d_6$) $\delta$ 0.83 (t, 9H), 1.16−1.28 (m, 4H), 1.35 (s, 9H), 1.30−1.44 (m, 4H), 1.48−1.58 (m, 1H), 2.90−3.10 (m, 2H), 3.80−3.96 (m, 1H), 6.75 (d, $J$ = 8.5 Hz, 1H), 7.68 (t, 1H); $m/z$ (LCMS, ESI): found 301.1 $[M + H]^+$, $[C_{16}H_{32}N_2O_3 + H]^+$ requires 301.2.

*(S)-2-(tert-Butoxycarbonylamino)-N-isopentyl-4-methylpentanamide (**i9b**).* Following the general procedure for amide coupling, Boc-L-leucine (578 mg, 2.5 mmol) was reacted with isoamylamine (262 mg, 3.0 mmol) in anhydrous DMF (10 mL), using PyBop as a coupling reagent (1.56 g, 3.0 mmol) and diisopropylethylamine (1.07 g, 8.25 mmol) as a base. A 555 mg amount of compound **i9b** was obtained after purification with flash chromatography (74%). $^1$H NMR (DMSO-$d_6$) $\delta$ 0.86 (d, 12H), 1.22−1.42 (m, 13H), 1.50−1.64 (m, 2H), 3.00−3.12 (m, 2H), 3.66−3.76 (m, 1H), 6.77 (d, $J$ = 8.5 Hz, 1H), 7.72 (t, 1H); $m/z$ (LCMS, ESI): found 323.1 $[M + Na]^+$, $[C_{16}H_{32}N_2O_3 + Na]^+$ requires 323.2.

*General Procedure for Boc Deprotection. Intermediate **j5a**, **j9a**, **j5a**, and **j9b**.* The Boc-protected compound was dissolved either in 3 M HCl/MeOH or in ethyl acetate. When the compound is dissolved into ethyl acetate, hydrogen chloride gas generated from the reaction of sulfuric acid and sodium chloride was bubbled into the solution at 0 °C. The solution was then stirred for 1.5−3 h at room temperature when HCl/MeOH solution is used or at 0 °C when HCl is bubbled into the solution. The volatile materials were then removed under vacuum to give the product as hygroscopic solid which was purified with reverse phase HPLC.

*L-Leucinyl-L-norleucine Methyl Ester Hydrochloride (**j5a**).* Following the general procedure for Boc deprotection, compound **i5a** (537 mg, 1.5 mmol) was exposed to 3 M HCl/MeOH (3.0 mL) for 3 h. A 423 mg amount of compound **j5a** was obtained after purification with reverse phase HPLC (96%). $^1$H NMR (DMSO-$d_6$) $\delta$ 0.82−0.94 (m, 9H), 1.22−1.36 (m, 4H), 1.48−1.60 (m, 2H), 1.60−1.76 (m, 3H), 3.61 (s, 3H), 3.79 (t, 1H), 4.22−4.30 (m, 1H), 8.29 (brs, 3H), 8.88 (d, $J$ = 7.2 Hz, 1H); $m/z$ (LCMS, ESI): found 259.2 $[M + H]^+$, $[C_{13}H_{26}N_2O_3 + H]^+$ requires 259.2.

*((S)-2-Amino-4-methylpentanoyl)-L-leucine Methyl Ester Hydrochloride (**j9a**).* Following the general procedure for Boc deprotection, compound **i9a** (626 mg, 1.75 mmol) was exposed to 3 M HCl/MeOH (3.0 mL) for 2 h. A 506 mg amount of compound **j9a** was obtained after purification with reverse phase HPLC (98%). $^1$H NMR (DMSO-$d_6$) $\delta$ 0.82−0.96 (m, 12H), 1.45−1.66 (m, 4H), 1.66−1.78 (m, 2H), 3.62 (s, 3H), 3.83 (t, $J$ = 7.0 Hz, 1H), 4.26−4.34 (m, 1H), 8.45 (brs, 3H), 9.05 (d, $J$ =7.5 Hz, 1H); $m/z$ (LCMS, ESI): found 259.1 $[M + H]^+$, $[C_{13}H_{26}N_2O_3 + H]^+$ requires 259.2.

*(S)-2-Amino-4-methyl-N-pentylpentanamide Hydrochloride (**j5b**).* Following the general procedure for Boc deprotection,

compound **i5b** (450 mg, 1.5 mmol) was exposed to 3 M HCl/MeOH (3.0 mL) for 2 h. A 340 mg amount of compound **j5b** was obtained after purification with reverse phase HPLC (96%). $^1$H NMR (DMSO-$d_6$) $\delta$ 0.80−0.9 (m, 9H), 1.18−1.30 (m, 4H), 1.36−1.46 (m, 2H), 1.49−1.63 (m, 3H), 2.97−3.06 (m, 1H), 3.09−3.18 (m, 1H), 3.67 (t, 1H), 8.26 (brs, 3H), 8.59 (t, $J$ = 5.2 Hz, 1H); $m/z$ (LCMS, ESI): found 201.1 $[M + H]^+$, $[C_{11}H_{24}N_2O + H]^+$ requires 201.2.

*(S)-2-Amino-N-isopentyl-4-methylpentanamide Hydrochloride (**j9b**).* Following the general procedure for Boc deprotection, compound **i9b** (450 mg, 1.5 mmol) was exposed to 3 M HCl/MeOH (3.0 mL) for 3 h. A 340 mg amount of compound **j9b** was obtained after purification with reverse phase HPLC (96%). $^1$H NMR (DMSO-$d_6$) $\delta$ 0.82−0.92 (m, 12H), 1.28−1.38 (m, 2H), 1.53−1.66 (m, 4H), 3.02−3.10 (m, 1H), 3.12−3.20 (m, 1H), 3.68−3.76 (m, 1H), 8.38 (brs, 3H), 8.75 (t, $J$ = 5.5 Hz, 1H); $m/z$ (LCMS, ESI): found 223.1 $[M + Na]^+$, $[C_{11}H_{24}N_2O + Na]^+$ requires 223.2.

*General Procedure for the Synthesis of Compounds **1a**−**12a** and **1b**−**12b**.* To a cooled solution of compound **4** (1 equiv), any of compounds **j1a**−**j12a** or **j1b**−**j12b** (1.2−1.5 equiv), and PyBop (1.2 equiv) in anhydrous DCM was added diisopropylethylamine (4 equiv) gradually. The reaction mixture was stirred at rt for 6 h to overnight. The reaction mixture was then diluted with DCM up to 25 mL; extracted with 5% citric acid (2 × 12 mL), saturated sodium bicarbonate (2 × 12 mL), and brine (2 × 10 mL); and dried over anhydrous sodium sulfate. The solvent was then evaporated under reduced pressure, and the residue was purified by semipreparative HPLC to give the intermediate that corresponds to the starting **j1a**−**j12a** or **j1b**−**j12b** compound among **k1a**−**k12a** and **k1b**−**k12b**. This intermediate was then hydrolyzed in the following manner: 0.2 mmol of this intermediate was vigorously shaken at room temperature with 1−2 mL of 0.4 M LiOH aqueous solution until all the solid dissolves (acetonitrile was used as a cosolvent whenever needed). The solution was then stirred for 2− 24 h and concentrated under vacuum. The final compound was then separated as a pure lithium or dilithium salt using semipreparative reverse phase HPLC.

*Dilithium ((S)-2-((N-(Benzyloxycarbonyl)-aminomethylphosphonyl)amino)-4-methylpentanoyl)-L-norleucinate (**5a**).* Following the general procedure for the synthesis of compounds **5a**, **9a**, **5b**, and **9b**, compound **4** (215 mg, 0.83 mmol) was reacted with compound **j5a** (295 mg, 1.0 mmol) in anhydrous DCM (3.0 mL), using PyBop (520 mg, 1.0 mmol) as a coupling reagent and diisopropylethylamine (428 mg, 3.3 mmol) as a base. A 281 mg amount of compound **k5a**, which is the diester version of the desired product, was obtained after purification with reverse phase HPLC (68%). A 100 mg amount of this compound (0.2 mmol) was then exposed to LiOH (2.0 mL of the 0.4 M solution referred to in the general procedure; 2.0 mL of acetonitrile was used as a cosolvent) overnight, and the final product was separated by reverse phase HPLC as a pure white solid (91 mg, 95%). $^1$H NMR ($D_2O$) $\delta$ 0.68−0.80 (m, 9H), 1.08−1.20 (m, 4H), 1.25−1.42 (m, 2H), 1.49−1.70 (m, 3H), 3.08−3.22 (m, 2H), 3.50−3.58 (m, 1H), 4.01 and 4.02 (2 d, $J$ = 7.6 Hz, together 1H), 4.99 (s, 2H), 7.24−7.36 (m, 5H), $^{31}$P NMR ($D_2O$) $\delta$ 17.50; $m/z$ (LCMS, ESI): found 478.3 $[M - Li + 2H]^+$; $[C_{21}H_{32}Li_2N_3O_7P - Li + 2H]^+$ requires 478.2.

*Dilithium ((S)-2-((N-(Benzyloxycarbonyl)-aminomethylphosphonyl)amino)-4-methylpentanoyl)-L-leucinate (**9a**).* Following the general procedure for the synthesis of compounds **5a**, **9a**, **5b**, and **9b**, compound **4** (130 mg, 0.5 mmol) was reacted with compound **j9a** (221 mg, 0.75 mmol) in anhydrous DCM (3.0 mL), using PyBop (312 mg, 0.6 mmol) as a coupling reagent and diisopropylethylamine (258 mg, 2.0 mmol) as a base. A 177 mg amount of compound **k9a**, which is the diester version of the desired product, was obtained after purification with reverse phase HPLC (71%). A 100 mg amount of this compound (0.2 mmol) was then exposed to LiOH (2.0 mL of the 0.4 M solution referred to in the general procedure; an additional 2.0 mL of acetonitrile was used as a cosolvent) for 10 h, and the final product was separated by reverse phase HPLC as a pure white solid (78 mg, 81%). $^1$H NMR ($D_2O$) $\delta$ 0.66−0.78 (m, 12H), 1.23−1.58 (m, 6H), 3.04−3.20 (m, 2H), 3.49−3.57 (m, 1H), 4.02−4.08 (m, 1H), 4.97 (s, 2H), 7.20−7.34 (m, 5H); $^{13}$C NMR ($D_2O$) $\delta$ 21.19, 21.55, 22.54, 22.69, 24.20, and 24.79 (6C, 2$\underline{C}$H($\underline{C}$H$_3$)$_2$), 40.04 (d, $J_{C-P}$ = 543 Hz, 1C, $\underline{C}$H$_2$P), 41.22, 43.64, and 43.71 (2C, 2$\underline{C}$H$_2$CH(CH$_3$)$_2$), 54.00 and 54.32 (2C, 2$\underline{C}$HCO), 67.32 (1C, Ph$\underline{C}$H$_2$O−), 128.01, 128.60, 129.02, and 136.66 (6C, Ph), 158.41 (1C, Cbz $\underline{C}$═O), 177.44 and 179.96 (2C, 2$\underline{C}$═O), $^{31}$P NMR ($D_2O$) $\delta$ 17.45; $m/z$ (LCMS, ESI): found 470.3 $[M - 2Li + H]^-$; $[C_{21}H_{32}Li_2N_3O_7P - 2Li + H]^-$ requires 470.2.

*(S)-2-((N-(Benzyloxycarbonyl)aminomethylphosphonyl)amino)-4-methyl-N-pentylpentanamide Lithium (**5b**).* Following the general procedure for the synthesis of compounds **5a**, **9a**, **5b**, and **9b**, compound **4** (215 mg, 0.83 mmol) was reacted with compound **j5b** (237 mg, 1.0 mmol) in anhydrous DCM (3.0 mL), using PyBop (520 mg, 1.0 mmol) as a coupling reagent and diisopropylethylamine (428 mg, 3.3 mmol) as a base. A 274 mg amount of compound **k5b**, which is the PO-methyl ester version of the desired product, was obtained after purification with reverse phase HPLC (75%). A 88 mg amount of this compound (0.2 mmol) was then exposed to LiOH (1.5 mL of the 0.4 M solution referred to in the general procedure; an additional 1.5 mL of acetonitrile was used as a cosolvent) overnight, and the final product was separated by reverse phase HPLC as a pure white solid (62 mg, 72%). $^1$H NMR ($D_2O$) $\delta$ 0.68−0.78 (m, 9H), 1.05−1.10 (m, 4H), 1.22−1.40 (m, 4H), 1.45−1.55 (m, 1H), 2.98 (t, $J$ = 6.4 Hz, 2H), 3.00−3.20 (m, 2H), 3.45−3.52 (m, 1H), 4.99 (s, 2H), 7.22−7.36 (m, 5H), $^{31}$P NMR ($D_2O$) $\delta$ 17.29; $m/z$ (LCMS, ESI): found 428.2 $[M - Li + 2H]^+$; $[C_{20}H_{33}LiN_3O_5P - Li + 2H]^+$ requires 428.2.

*(S)-2-((N-(Benzyloxycarbonyl)aminomethylphosphonyl)amino)-N-isopentyl-4-methylpentanamide Lithium (**9b**).* Following the general procedure for the synthesis of compounds **5a**, **9a**, **5b**, and **9b**, compound **4** (215 mg, 0.83 mmol) was reacted with compound **j9b** (237 mg, 1.0 mmol) in anhydrous DCM (3.0 mL), using PyBop (520 mg, 1.0 mmol) as a coupling reagent and diisopropylethylamine (428 mg, 3.3 mmol) as a base. A 245 mg amount of compound **k9b**, which is the PO-methyl ester version of the desired product, was obtained after purification with reverse phase HPLC (67%). A 88 mg amount of this compound (0.2 mmol) was then exposed to LiOH (1.5 mL of the 0.4 M solution referred to in the general procedure; an additional 1.5 mL of acetonitrile was used as a cosolvent) overnight, and the final product was separated by reverse phase HPLC as a pure white solid (78 mg, 90%). $^1$H NMR ($CD_3OD$) $\delta$ 0.88−0.98 (m, 12H), 1.38−1.46 (m, 3H), 1.54−1.68 (m, 2H), 1.75−1.83 (m, 1H), 3.18−3.32 (m, 4H), 3.68−3.74 (m, 1H), 5.10 (s, 2H), 7.28−7.42 (m, 5H), $^{13}$C NMR ($CD_3OD$) $\delta$ 21.53, 21.86, 21.88, 22.54, 24.68, and 25.95 (6C, 2$\underline{C}$H($\underline{C}$H$_3$)$_2$), 37.72 and 38.29 (2C, 2$\underline{C}$H$_2$CH(CH$_3$)$_2$), 40.73 (d, $J_{C-P}$ = 543 Hz, 1C, $\underline{C}$H$_2$P), 44.22 and 44.29 (1C, HN$\underline{C}$H$_2$CH$_2$), 54.51 (1C, $\underline{C}$HCONH), 66.69 (1C, Ph$\underline{C}$H$_2$O), 127.89, 128.01, 128.47, and 137.28 (6C, Ph), 158.0 (1C, Cbz $\underline{C}$═O), 177.05 (1C, $\underline{C}$═O), $^{31}$P NMR ($CD_3OD$) $\delta$ 15.75; $m/z$ (LCMS, ESI): found 440.3 and 873.5 $[M + Li]^+$ and $[2 M + Li]^+$; $[C_{20}H_{33}LiN_3O_5P + Li]^+$ requires 440.2.

**ITC, X-ray Crystallography, and Molecular Modeling.** Details of the experimental procedures of ITC are provided in the Supporting Information. The crystal structures of the complexes of thermolysin with **1a**, **2a**, **3a**, **4a**, **6a**, **8a**, **9a**, **11a**, **1b**, and **2b** were previously reported under PDB IDs 3T8G, 3T74, 3T87, 3T8C, 3T8H, 3T8D, 4H57, 4D9W, 3T73, and 3T8F. Molecular modeling experiments were carried out on some of the ligands that do not have crystal structures (e.g., **3b**, **4b**, **6b**, **7a**, and **7b**). The purpose of these experiments was to predict the potential binding modes of the P2′ side chains of these ligands in the ligand−protein complexes. The steric compatibility, as well as the interactions between a modeled P2′ side chain and the hydration water structures observed in the crystallographic complexes of ligands with smaller P2′ side chains, could then be investigated (e.g., the position of the side chain of **3b** relative to the hydration waters observed in the crystal structure of the **2b**−TLN complex). All the modeling experiments described herein were performed using SYBYL-X software; Tripos Inc. Modeling experiments were performed according to the following protocol:

Either the crystal structure, for which the relative position of the modeled side chain was to be compared with (e.g., that of ligand **2b**; PDB ID: 3T8F), or a model system of the active site constructed based on this crystal structure was used for the modeling experiment.

First, this crystal structure was downloaded and used to construct the model system if necessary. The hydrogen atoms were added to both the ligand and the protein. The atom and bond types as well as the protonation status for the ligand and the active site residues were checked and repaired when necessary. Gasteiger–Huckel charges for the ligand and the water molecules, and Kollman-all atom charges for the protein as well as the zinc and calcium ions were then calculated. This was followed by minimizing the added hydrogen atoms with Tripos force field using the default parameters with the exception of using the charges that were previously loaded on the ligand–protein complex atoms, and using a value of 80 for the dielectric constant. It should be noted that during this minimization procedure, all the heavy atoms were kept constrained in order not to lose the crystallographic information (the ligand binding mode, the positions of the water molecules, etc.).

Second, a duplicate pdb file of the previously prepared structure was generated. All the hydration water molecules were then removed and the P2′ side chain under investigation was constructed from the original side chain in multiple conformations (e.g., the Me side chain of ligand **2b** was extended to an ethyl, producing ligand **3b**; multiple conformations were generated by torsion angle rotations). Hydrogen atoms were added to the constructed side chain, and the partial charges were recalculated in the manner previously described (i.e., Gasteiger–Huckel charges for the ligand and Kollman-all atom charges for the protein). The new P2′ side chain and all the hydrogen atoms were then minimized using Tripos force field, while keeping the remaining ligand and protein atoms constrained (note: side chains of protein residues were include in the minimization process whenever they were in steric clashes with the ligand's newly constructed P2′ side chain).

Finally, the structure with the newly constructed P2′ side chain (i.e., the modeled ligand) was superimposed on the crystallographic complex of the reference ligand (e.g., the modeled structure of the **3b**–TLN was superimposed on the crystallographic complex of **2b** with TLN). The coordinates of the ligand of the crystallographic complex were used to guide the superimposition process. The steric compatibility of the P2′ side chain of the modeled ligand with the hydration waters and the protein residues of the crystallographic complex was then determined and utilized in the discussions presented in this paper.

## ■ ASSOCIATED CONTENT

### Supporting Information

The experimental details of ligand synthesis (except ligands **5a**, **9a**, **5b**, and **9b**) and ITC (with isotherms' pictures and a table including the observed thermodynamic data), as well as supplementary figures and discussions. This material is available free of charge via the Internet at http://pubs.acs.org.

## ■ AUTHOR INFORMATION

### Corresponding Authors

*(D.H.) E-mail: hangauer@buffalo.edu. Phone: 716-898-8617. *(N.N.N.) E-mail: nnnasief@yahoo.com. Phone: 716-881-8919.

### Notes

The authors declare no competing financial interest.

## ■ ACKNOWLEDGMENTS

The first author thanks Prof. Andrew Murkin, the Department of Chemistry, University at Buffalo, The State University of New York, Buffalo, for training him on the VP-ITC instrument. We also thank him for his suggestion to additionally confirm the purity of some of the ligands using NMR in the presence of imidazole as an internal standard.

## ■ ABBREVIATIONS USED

Bn, benzyl; *i*-Bu, isobutyl; *n*-Bu, normal butyl; *sec*-Bu, secondary butyl; *tert*-Bu, tertiary butyl; Et, ethyl; eq, equation; ITC, isothermal titration calorimetry; Me, methyl; MUP, major urinary protein; *i*-Pr, isopropyl; *n*-Pr, normal propyl; TLN, thermolysin

## ■ REFERENCES

(1) Kauzmann, W. Some factors in the interpretation of protein denaturation. *Adv Protein Chem.* **1959**, *14*, 1–63.
(2) Tanford, C. The hydrophobic effect and the organization of living matter. *Science* **1978**, *200*, 1012–1018.
(3) Graziano, G. Hydration entropy of polar, nonpolar and charged species. *Chem. Phys. Lett.* **2009**, *479*, 56–59.
(4) Graziano, G. Scaled particle theory study of the length scale dependence of cavity thermodynamics in different liquids. *J. Phys. Chem. B* **2006**, *110*, 11421–11426.
(5) Graziano, G.; Lee, B. Entropy convergence in hydrophobic hydration: a scaled particle theory analysis. *Biophys. Chem.* **2003**, *105*, 241–250.
(6) Lemieux, R. U. How water provides the impetus for molecular recognition in aqueous solution. *Acc. Chem. Res.* **1996**, *29*, 373–380.
(7) Bingham, R. J.; Findlay, J. B. C.; Hsieh, S.-Y.; Kalverda, A. P.; Kjellberg, A.; Perazzolo, C.; Phillips, S. E. V.; Seshadri, K.; Trinh, C. H.; Turnbull, W. B.; Bodenhausen, G.; Homans, S. W. Thermodynamics of binding of 2-methoxy-3-isopropylpyrazine and 2-methoxy-3-isobutylpyrazine to the major urinary protein. *J. Am. Chem. Soc.* **2004**, *126*, 1675–1681.
(8) Homans, S. W. Water, water everywhere-except where it matters. *Drug Discovery Today* **2007**, *12*, 534–539.
(9) Snyder, P. W.; Mecinovic, J.; Moustakas, D. T.; Tomas, S. W., III; Harder, M.; Mack, E. T.; Lockett, M. R.; Heroux, A.; Sherman, W.; Whitesides, G. M. Mechanism of the hydrophobic effect in the biomolecular recognition of arylsulfonamides by carbonic anhydrase. *Proc. Natl. Acad. Sci. U.S.A.* **2011**, *108*, 17889–17894.
(10) Mecinovic, J.; Snyder, P. W.; Mirica, K. A.; Bai, S.; Mack, E. T.; Kwant, R. L.; Moustakas, D. T.; Heroux, A.; Whitesides, G. M. Fluoroalkyl and alkyl chains have similar hydrophobicities in binding to the "hydrophobic wall" of carbonic anhydrase. *J. Am. Chem. Soc.* **2011**, *133*, 14017–14026.
(11) Englert, L.; Biela, A.; Zayed, M.; Heine, A.; Hangauer, D.; Klebe, G. Displacement of disordered water molecules from hydrophobic pocket creates enthalpic signature: Binding of phosphonamidate to the $S_1'$-pocket of thermolysin. *Biochim. Biophys. Acta* **2010**, *1800* (11), 1192–1202.
(12) Latt, S. A.; Holmquist, B.; Vallee, B. L. Thermolysin: A zinc metalloenzyme. *Biochem. Biophys. Res. Commun.* **1969**, *37*, 333–339.
(13) Morihara, K.; Tsuzuki, H. Thermolysin: kinetic study with oligopeptides. *Eur. J. Biochem.* **1970**, *15*, 374–380.
(14) Hangauer, D. G.; Monzingo, A. F.; Matthews, B. W. An interactive computer graphics study of thermolysin-catalyzed peptide cleavage and inhibition by *N*-carboxymethyl dipeptides. *Biochemistry* **1984**, *23*, 5730–5741.
(15) Biela, A.; Nasief, N. N.; Betz, M.; Heine, A.; Hangauer, D.; Klebe, G. Dissecting the hydrophobic effect on molecular level: The role of water, enthalpy and entropy in ligand binding to thermolysin. *Angew. Chem., Int. Ed.* **2013**, *52*, 1822–1828.
(16) Nasief, N. N.; Tan, H.; Kong, J.; Hangauer, D. Water mediated ligand functional group cooperativity: The contribution of a methyl group to binding affinity is enhanced by a $COO^-$ group through changes in the structure and thermodynamics of the hydration waters of ligand–thermolysin complexes. *J. Med. Chem.* **2012**, *55*, 8283–8302.
(17) Holdgate, G. A. Making cool drugs hot: Isothermal titration calorimetry as a tool to study binding energetics. *BioTechniques.* **2001**, *31*, 164–166.

(18) Perozzo, R.; Folkers, G.; Scapozza, L. Thermodynamics of protein-ligand interactions: history, presence, and future aspects. *J. Recept. Signal Transduct. Res.* **2004**, *24*, 1−52.
(19) Freire, E. A thermodynamic approach to the affinity optimization of drug candidates. *Chem. Biol. Drug Des.* **2009**, *74*, 468−472.
(20) Ladbury, J. E. Calorimetry as a tool for understanding biomolecular interactions and an aid to drug design. *Biochem. Soc. Trans.* **2010**, *38*, 888−893.
(21) Tellinghuisen, J.; Chodera, J. D. Systematic errors in isothermal titration calorimetry: Concentrations and baselines. *Anal. Biochem.* **2011**, *414*, 297−299.
(22) Myszka, D. G.; Abdiche, Y. N.; Arisaka, F.; Byron, O.; Eisenstein, E.; et al. The ABRF-MIRG'02 study: assembly state, thermodynamic, and kinetic analysis of an enzyme/inhibitor interaction. *J. Biomol. Tech.* **2009**, *14*, 247−269.
(23) Chodera, J. D.; Mobley, D. L. Entropy-enthalpy compensation: Role and ramifications in biomolecular ligand recognition and design. *Annu. Rev. Biophys.* **2013**, *42*, 121−142.
(24) The crystallographic data of **3a** (PDB ID: 3T87), **4a** (PDB ID: 3T8C), **6a** (PDB ID: 3T8H), **8a** (PDB ID: 3T8D), **9a** (PDB ID: 4H57), and **11a** (PDB ID: 4D9W), which are employed in the discussion section of this paper, were previously published in ref 15. The crystal structures of **1a**, **2a**, **1b**, and **2b** were discussed in ref 16, and are reported under PDB IDs 3T8G, 3T74, 3T73, and 3T8F.
(25) Lum, K.; Chandler, D.; Weeks, J. D. Hydrophobicity at small and large length scales. *J. Phys. Chem. B* **1999**, *103*, 4570−4577.
(26) Southall, N. T.; Dill, K. A. The mechanism of hydrophobic solvation depends on solute radius. *J. Phys. Chem. B* **2000**, *104*, 1326−1331.
(27) Chandler, D. Interfaces and the driving force of hydrophobic assembly. *Nature* **2005**, *437*, 640−647.
(28) Dill, K. A.; Truskett, T. M.; Vlachy, V.; Hribar-Lee, B. Modeling water, the hydrophobic effect, and ion salvation. *Annu. Rev. Biophys. Biomol. Struct.* **2005**, *34*, 173−199.
(29) Garde, S.; Patel, A. J. Unraveling the hydrophobic effect, one molecule at a time. *Proc. Natl. Acad. Sci. U.S.A.* **2011**, 16491−16492.
(30) Suzuki, S.; Green, P. G.; Bumgarner, R. E.; Suenram, F. J.; Lovas, S.; Dasgupta, S.; Goddard, W. A., III; Blake, G. A. Benzene forms hydrogen bonds with water. *Science* **1992**, *257*, 942−945.
(31) Steiner, T. Hydrogen bonds from water molecules to aromatic acceptors in very high-resolution protein crystal structures. *Biophys. Chem.* **2002**, *95*, 195−201.
(32) Gierszal, K. P.; Davis, J. G.; Hands, M. D.; Wilcox, D. S.; Slipchenko, L. V.; Ben-Amotz, D. $\pi$-Hydrogen bonding in liquid water. *J. Phys. Chem. Lett.* **2011**, *2*, 2930−2933.
(33) Velazquez-Campoy, A.; Todd, M. J.; Freire, E. HIV-1 Protease inhibitors: enthalpic versus entropic optimization of the binding affinity. *Biochemistry* **2000**, *39*, 2201−2207.
(34) Freire, E. Do enthalpy and entropy distinguish first in class from best in class? *Drug Discovery Today* **2008**, *13*, 869−874.
(35) Ladbury, J. E.; Klebe, G.; Freire, E. Adding calorimetric data to decision making in lead discovery: A hot tip. *Nat. Rev. Drug Discovery* **2010**, *9*, 23−27.
(36) Reynolds, C. H.; Holloway, M. K. Thermodynamics of ligand binding and efficiency. *ACS Med. Chem. Lett.* **2011**, *2*, 433−437.
(37) Vo-Quang, Y.; Gravey, A. M.; Simonneau, R.; Vo-Quang, L.; Lacoste, A. M.; Le Goffic, F. Towards new inhibitors of D-alanine:D-alanine ligase: The synthesis of 3-amino butenylphosphonic and aminophosphonamidic acids. *Tetrahedron Lett.* **1987**, *28*, 6167−6170.

## ■ NOTE ADDED IN PROOF

After the submission of this paper, we noticed a remarkable study which just appeared in the literature reporting the existence of enthalpy−entropy compensation in the binding of human carbonic anhydrase (HCA) to a series of benzothiazole sulfonamide ligands (Breiten, B.; Lockett, M. R.; Sherman, W.; Fujita, S.; Al-Sayah, M.; Lange, H.; Bowers, C. M.; Heroux, A.; Krilov, G.; Whitesides, G. M. Water networks contribute to enthalpy/entropy compensation in protein−ligand binding. *J. Am. Chem. Soc.* **2013**, *135*, 15579−15584). Bearing in mind that the current paper distinctively explores the neighboring group effect on the thermodynamics of the hydrophobic binding, both the current and the reported papers suggest similar water-centric views to explain the enthalpy−entropy compensations observed in the binding of TLN and HCA to the phosphonamidate and the sulfonamide ligands, respectively.